

1. EXPLANATORY NOTES¹

Shipboard Scientific Party²

INTRODUCTION

This chapter is devoted to a description of the sampling, measurement, and core description procedures and methods used during Leg 140. It will help the reader to understand the basis for our preliminary conclusions and also help the interested investigator select samples for further analysis. This chapter concerns only shipboard operations and analyses described in the site report in the *Initial Reports* volume of the Leg 140 *Proceedings of the Ocean Drilling Program*. Methods used by various investigators for shore-based analysis of Leg 140 data will be detailed in individual papers published in the *Scientific Results* volume.

Site Chapter

Descriptions of individual drilling sites, summaries of operations, and preliminary results are contained in the site chapter. The separate sections of the site chapter were written by the following shipboard scientists (authors are listed in alphabetical order; no seniority is implied):

Site Summary: Dick, Erzinger
Background and Objectives: Dick, Erzinger
Operations: Pollard, Stokking
Petrography: Agrinier, Alt, Fisk, Johnson, Kelley, Kepezhinskas, Laverne, McNeill, Naslund, Schandl, Sparks, Umino, Vanko, Zuleger
Alteration and Metamorphism: Agrinier, Alt, Kelley, Laverne, Schandl, Vanko, Zuleger
Geochemistry: Agrinier, Fisk, Johnson, Kepezhinskas, Sparks, Zuleger
Structure and Deformation: Allerton, Marton, McNeill, Pertsev, Tartarotti
Paleomagnetism: Allerton, Pariso, Stokking
Physical Properties: Boldreel, Harvey, Iturrino, Pezard
Downhole Measurements: Boldreel, Harvey, Iturrino, Pezard
Lithostratigraphic Summary: Dick, Erzinger
Summary and Conclusions: Dick, Erzinger
Appendix: Shipboard Scientific Party

Following the text of the site chapter are summary core descriptions (visual core descriptions for igneous and metamorphic rocks), thin-section descriptions, and photographs of each core.

Shipboard Scientific Procedures

Numbering of Sites, Holes, Cores, and Samples

Drilling sites are numbered consecutively from the first site drilled by the *Glomar Challenger* in 1968. A site number refers to one or more holes drilled while the ship was positioned over one acoustic beacon. Multiple holes may be drilled at a single site by pulling the drill pipe above the seafloor (out of the hole), moving the ship some distance from the previous hole, and then drilling another hole. In some cases, the ship may return to a previously occupied site to drill

additional holes or to log or deepen a previously existing hole, such as Hole 504B.

For all ODP drill sites, a letter suffix distinguishes each hole drilled at the same site. For example, the first hole drilled is assigned the site number modified by the suffix A, the second hole takes the site number and suffix B, and so forth. Note that this procedure differs slightly from that used by DSDP (Sites 1 through 624), but prevents ambiguity between site- and hole-number designations. It is important to distinguish among holes drilled at a site, because recovered rocks from different holes usually do not come from equivalent positions in the stratigraphic column.

The cored interval is measured in meters below seafloor (mbsf); sub-bottom depths are determined by subtracting the drill pipe measurement (DPM) water depth (the length of pipe from the rig floor to the seafloor) from the total DPM (from the rig floor to the bottom of the hole; see Fig. 1). Water depths below sea level can be determined by subtracting the height of the rig floor above sea level from the DPM water depth. The rig-floor height varies from site to site, and is given in the hole, depth, and location summary tables in each site report. Echo-sounding data (from the precision depth recorders) are used to locate the site, but they are not usually used as a basis for any further measurements. A water depth of 3460 m, determined on previous legs by echo sounding, is used in the Leg 140 *Initial Reports* in order to be consistent with depths reported from previous visits to Hole 504B.

The depth interval assigned to an individual core begins with the depth below the seafloor that the coring operation began, and extends to the depth that the coring operation ended for that core (see Fig. 1). For rotary coring (RCB), each coring interval is equal to the length of the joint of drill pipe added for that interval (though a shorter core may be attempted in special instances). The drill pipe in use varies from about 9.4 to 9.8 m. The pipe is measured as it is added to the drill string, and the cored interval is usually recorded as the length of the pipe joint to the nearest 0.1 m.

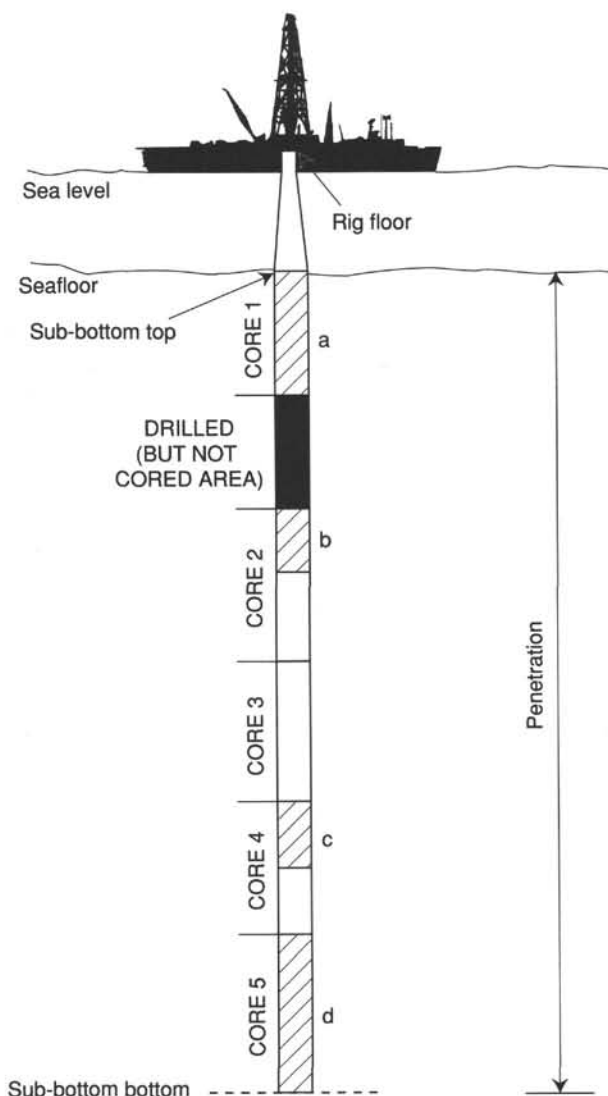
Cored intervals may not necessarily be adjacent if separated by drilled intervals. In soft material, the drill string can be "washed ahead" with the core barrel in place, without recovering anything. This is achieved by pumping water down the pipe at high pressure to wash the soft material out of the way of the bit and up the annulus between the drill pipe and the wall of the hole. If thin, hard layers are present, then it is possible to get "spotty" sampling of these resistant layers within the washed interval, and thus to have a cored interval greater than 9.5 m. In practice, this is rare and did not occur during Leg 140.

Cores taken from a hole are numbered serially from the top of the hole downward. Core numbers and their associated cored intervals (in mbsf) are unique in a given hole. Maximum full recovery for a single core is 9.5 m of rock contained in a plastic liner (6.6 cm internal diameter) plus about 0.2 m (without a plastic liner) in the core catcher (Fig. 2). The core catcher is a device at the bottom of the core barrel that prevents the core from sliding out when the barrel is being retrieved from the hole.

Each recovered core is divided into 1.5-m sections that are numbered serially from the top (Fig. 2); individual pieces of rock are then each assigned a number. Fragments of a single piece are assigned a single number, and individual fragments are identified alphabetically. When full recovery is obtained, the sections are numbered from 1

¹ Dick, H.J.B., Erzinger, J., Stokking, L.B., et al., 1992. *Proc. ODP, Init. Repts.*, 140: College Station, TX (Ocean Drilling Program).

² Shipboard Scientific Party is as given in the list of participants preceding the contents.



Represents recovered material

BOTTOM FELT: distance from rig floor to seafloor

TOTAL DEPTH: distance from rig floor to bottom of hole (sub-bottom bottom)

PENETRATION: distance from seafloor to bottom of hole (sub-bottom bottom)

NUMBER OF CORES: total of all cores recorded, including cores with no recovery

TOTAL LENGTH OF CORED SECTION: distance from sub-bottom top to sub-bottom bottom minus drilled (but not cored) areas in between

TOTAL CORE RECOVERED: total from adding a, b, c, and d in diagram

CORE RECOVERY (%): equals TOTAL CORE RECOVERED divided by TOTAL LENGTH OF CORED SECTION times 100

Figure 1. Diagram illustrating terms used in the discussion of coring operations and core recovery.

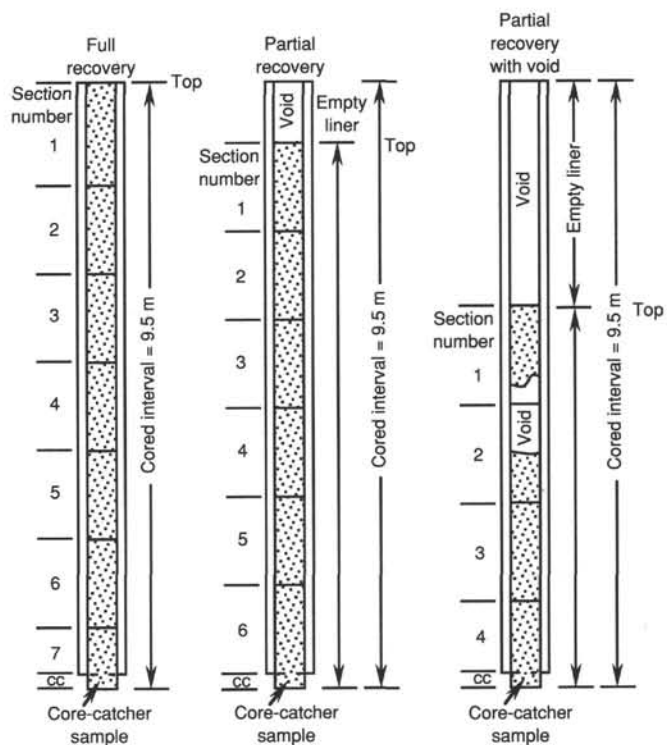


Figure 2. Diagram showing procedure used in cutting and labeling core sections.

through 7, with the last section possibly being shorter than 1.5 m (rarely, an unusually long core may require more than seven sections). When less than full recovery is obtained, there will be as many sections as needed to accommodate the length of the core recovered; for example, 4 m of core would be divided into two 1.5-m sections and one 1-m section. In rare cases a section less than 1.5 meters may be cut in order to preserve features of interest (e.g., lithological contacts). The core-catcher sample is placed at the bottom of the last section and is treated as part of the last section, rather than separately. Scientists completing visual core descriptions describe each lithologic unit, noting core and section boundaries only as physical reference points.

When, as is usually the case, the recovered core is shorter than the cored interval, the top of the core is equated with the top of the cored interval by convention, in order to achieve consistency in handling analytical data derived from the cores. Samples removed from the cores are designated by distance measured in centimeters from the top of the section to the top and bottom of each sample removed from that section. In curated hard-rock sections, sturdy plastic spacers are placed between pieces which did not fit together in order to protect them from damage in transit and in storage; therefore, the centimeter interval noted for a hard rock sample has no direct relationship to that sample's depth within the cored interval, but is only a physical reference to the location of the sample within the curated core.

A full identification number for a sample consists of the following information: leg, site, hole, core number, core type, section number, piece number (for hard rock), and interval in centimeters measured from the top of section. For example, a sample identification of "140-504B-186R-1, 10-12 cm" represents a sample removed from the interval between 10 and 12 cm below the top of Section 1, Core 186 (R designates that this core was taken during rotary coring) of Hole 504B during Leg 140.

All ODP core and sample identifiers indicate core type. The following abbreviations are used: R = Rotary Core Barrel (RCB); B = drill-bit recovery; I = in-situ water sample; W = wash-core recovery; and M = miscellaneous material. R and M cores were cut on Leg 140.

Core Handling

Igneous Rocks

Igneous rock cores are handled differently from sedimentary cores. Once on deck, the core catcher is placed at the bottom of the core liner, and total core recovery is calculated by shunting the rock pieces together and measuring to the nearest centimeter; this information is logged into the shipboard core-log database. If continuous lengths of hard rock greater than 20 cm are recovered, whole-round sections are run through the multisensor track (MST). The MST includes the GRAPE (gamma-ray attenuation porosity evaluator), *p*-wave logger, and magnetic susceptibility instrument. Generally, only GRAPE and susceptibility data are obtained from RCB cores, which are generally too disturbed to return useful *P*-wave data (see "Physical Properties" section, this chapter).

The core is then cut into 1.5-m-long sections and transferred into the lab. The contents of each section are transferred into 1.5-m-long sections of split core liner, where the bottoms of oriented pieces (i.e., pieces that clearly could not have rotated top to bottom about a horizontal axis in the liner) are marked with a red wax pencil. This is to ensure that orientation is not lost during the splitting and labeling process. To facilitate structural observations and measurements, a structural geologist marks each piece for splitting so that the principal structure dips parallel to the cut. The core is then split with a diamond saw into archive and working halves. A plastic spacer is used to separate individual pieces and/or reconstructed groups of pieces in the core liner. These spacers may represent a substantial interval of no recovery. Each piece is numbered sequentially from the top of each section, beginning with number 1; reconstructed groups of pieces are assigned the same number, but are lettered consecutively (e.g., 1A, 1B, 1C, etc.). Pieces are labeled only on external surfaces. If the piece is oriented, an arrow is added to the label pointing to the top of the section.

The archive half is drawn on the hard-rock visual core description form, noting size, shape, orientation, and special features of each piece (see "Petrography" section, this chapter). Most archive sections greater than 20 cm in length are run through the cryogenic magnetometer. The archive half is then photographed with both black-and-white and color film, one core at a time. Close-up photographs (black-and-white) are taken of particular features for illustrations in the summary of each site, as requested by the shipboard scientific party.

On Leg 140, the archive halves were described by three groups: igneous petrologists, metamorphic petrologists, and structural geologists. Separate core description logs were prepared by each group (see "Petrography," "Alteration and Metamorphism," and "Structure and Deformation" sections, this chapter). To ensure uniformity of measurements, a single individual was responsible for each kind of observation. The core was divided into igneous, metamorphic, and structural units, the boundaries of which do not necessarily coincide.

After the cores were described on Leg 140, the working halves were sampled for shipboard thin sections, physical properties, magnetic studies, X-ray fluorescence (XRF), and carbon-hydrogen-nitrogen-sulfur analyses. Analytical methods are described later in this chapter and the data are reported in the site chapter. Where recovery permitted, samples were taken from each lithologic unit for XRF analyses of major and selected trace elements. Additional samples were taken for XRF analyses from selected veins, shear zones, and alteration zones (see "Geochemistry" section, this chapter). Near the end of Leg 140, samples were taken from the working halves for shore-based laboratory studies. Each extracted sample was logged into the computer database by the location and the name of the investigator receiving the sample. The extracted samples were sealed in plastic vials or bags and labeled. Records of all samples are kept by the curator at ODP.

Both halves of the core are then shrink-wrapped in plastic to prevent rock pieces from vibrating out of sequence during transit, put

into labeled plastic tubes, sealed, and transferred to cold-storage space aboard the drilling vessel. All Leg 140 cores are housed in the Gulf Coast Repository.

OPERATIONS

Drilling Systems

The rotary core barrel (RCB) coring system (Fig. 3) used during Leg 140 has been the primary rock-recovery tool of the DSDP and ODP for many years. The RCB system can obtain representative core samples from many kinds of sediment or rock, and is the only known system that can core an entire sediment column of a kilometer or more and then core crystalline basement rocks without a bit change. The core is trimmed by the rotating cones of a roller-cone bit and must pass through the rotating bit throat before it enters the non-rotating inner core barrel. The core barrel and its plastic liner are decoupled from drill-string rotation by bearings at top and bottom. The cored interval is determined by the length of pipe added.

The bits normally used with the RCB system have four roller cones. The RCB bit diameter is 9-7/8 in. to 10-1/8 in., and the core throat diameter is 2-7/16 in. Because of the small opening and the use of a flapper-type check valve just above the bit, the bit must be dropped by using a mechanical bit release (MBR) before most logging or other tools can pass out of the drill string (see "Downhole Measurements" section, this chapter). A variety of tungsten carbide cutting structures are used on RCB bits, depending upon anticipated lithology. Longer, chisel-shaped inserts are used for gouging action in soft-to-medium material, whereas shorter chisel- or conical-shaped inserts are used to drill high-compressive-strength rocks through point loading. As a compromise, chisel inserts of medium length are used where lithology is varied or unknown. Operations on Leg 140 employed RCB bits specially hardened to increase rotating time from 15 to 20–30 hr per bit.

The RCB system differs from conventional oil-field coring in that the inner core barrels are wireline-retrievable. A special high-speed winch and 1/2 in. wire rope are used to retrieve the inner core barrel for each core, eliminating the need to trip the drill string. The choice of a coring system is determined by the nature of the material to be cored. If any considerable interval of lithified sediments and/or crystalline rocks is anticipated, the RCB system is generally used.

Drilling Characteristics

Drilling Parameters

Because water circulation in the borehole is open, cuttings are lost to the seafloor and cannot be examined. Information concerning lithologic stratification in uncored or unrecovered intervals may be inferred from seismic data, wireline-logging results, and from an examination of the behavior of the drill string as observed and recorded on the drilling platform. Typically, the harder a layer is, the slower and more difficult it is to penetrate. The driller must vary the parameters of weight-on-bit (WOB), rotations per minute (rpm), and circulation rate to produce the optimum outcome in terms of core recovery and rate of penetration (ROP). WOB may range from about 5000 lb in soft, shallow sediments to 40,000 lb in crystalline rocks, and depends upon the type of material being penetrated, the kind of bit in use, and the amount of drill-collar weight available to be applied to the bit. The drill string is usually rotated at 35–100 rpm, again depending on the type of bit and the nature of the "formation."

The parameters of rotary torque and circulating pressure are monitored to inform the driller of downhole conditions. An increase in the torque required to rotate the drill string may signal hole-cleaning problems, bit failure, or severe hole deviation. The fluid circulating pressure required is determined primarily by the length of the drill string and the amount of restriction at the bit. Changes in pressure may signal successful (or unsuccessful) latch-in

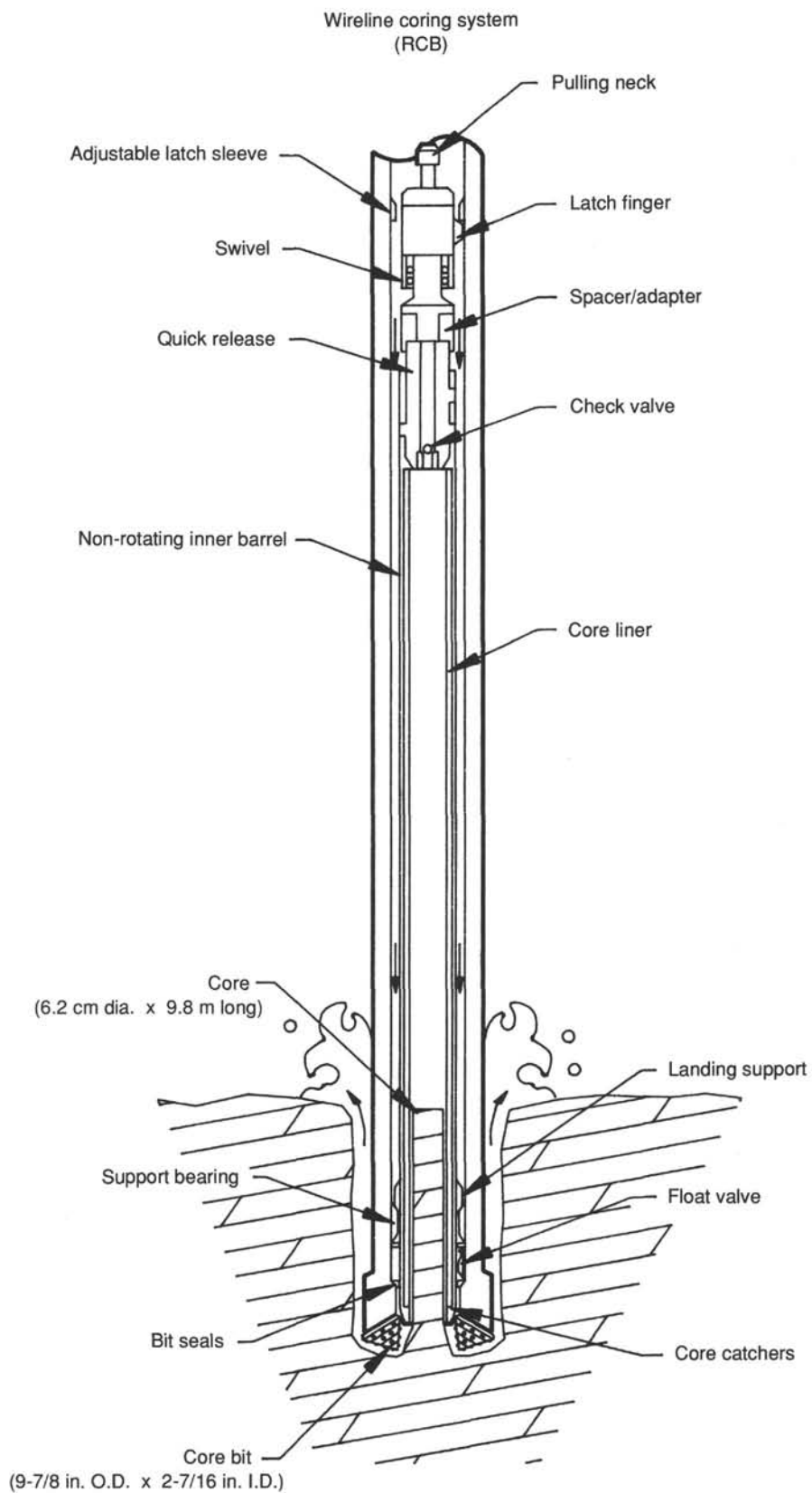


Figure 3. Rotary coring system.

of the inner barrel at the bit, hole-cleaning problems, or plugged bit nozzles.

The above parameters are recorded in analog form by the Martin-Decker drilling recorder on the drill floor; the records are available in the ODP Operations office.³ A computerized TOTCO drilling recorder system that will record drilling data digitally is being developed.

Drilling Deformation in Rotary Cores

Grooving

Core-catcher teeth, or "dogs," often cause continuous external marks, either longitudinal or spiral, on the cores. Longitudinal marks probably result from rock chips or debris behind one or more of the core-catcher dogs which prevented them from opening fully. Often, for unknown reasons, the RCB core barrel does not remain stationary with respect to the core but instead rotates with the outer barrel. The result is spiral grooving by the core-catcher dogs that resembles lathe machining. In some cases, a rather severe reduction in core diameter results.

Fracturing, Disintegration, and Discing

The proportion of core fracturing that results from drilling and coring processes is not known. Sometimes cores are recovered so severely fractured and broken that they literally fall apart when the liners are split. In some cases, the brittle failure of the core can be related to open fractures, strong veining, and/or paleotectonic textures. However, at greater depths, core discing, which does not correspond to fractures, veins, or textures is obvious. Discing breaks are perpendicular to the hole axis, and disk morphology is often buckled and saddle-shaped, with thicknesses of 1–10 cm. Different zones of stress concentration at the bottom of the borehole lead to core failure during drilling. Core discing, in-situ stress, and rock mechanical properties of the rocks are probably related. Core discing was frequently found in Leg 140 cores and is described in the site chapter.

PETROGRAPHY

Visual Core Description

Igneous and metamorphic visual core description (VCD) forms were used on Leg 140 (Fig. 4). The left column of the form is a graphic representation of the archive half. A horizontal line across the entire width of the column denotes a plastic spacer glued between rock pieces inside the liner. Oriented pieces are indicated on the form by an upward-pointing arrow to the right of the piece. Shipboard samples and studies are indicated on the VCD in the column headed "Shipboard Studies" using the following notation: X = X-ray fluorescence analysis; T = petrographic thin section; M = paleomagnetic analysis; and P = physical properties analysis. No X-ray diffraction equipment was available on board.

Igneous Rock Descriptions

Many of the rocks recovered during Leg 140 display a continuous range of grain sizes from fine to coarse so the division of samples into "fine-grained" and "coarse-grained," and to use separate description forms for the two groups, as has been done on some previous DSDP/ODP legs, would be somewhat arbitrary. The Igneous Data Logs used on Leg 140 were designed to accommodate the entire range of rock types expected. The igneous logs are described below.

1. The Igneous Contacts Log (Appendix A) identifies the location and type of contacts that define lithologic units. If a contact was recovered,

its location was recorded by core, section, position (cm), and piece number, and the overlying unit number is given. When a contact was not recovered but a change of lithology was observed, a contact was indicated at the base of the lowest piece in the overlying lithologic unit. The lithology of the overlying unit and the "character" of the contact are also listed. The lithology (rock name) was based on the Igneous Lithology Log; the character of the contact includes the contact type, as described in Figure 5, and a brief description of the contact. Strike, dip, and azimuth of each contact are recorded, if available.

2. The Igneous Lithology Log (Appendix B) was used to record the core, section, pieces, and cm interval for each unit as defined by the contacts. Lithology (rock name) and igneous textures were also recorded. Fabric orientation, color, percent vesicles, percent oxide minerals, and percent sulfide minerals as observed in the hand specimens are also entered. A list of possible rock textures are given in Table 1. If a fabric was evident, its orientation and strength (MacCaskie, 1986) is indicated. Nonplanar fabrics are indicated by "flow alignment." Color is that of the cut surface of the dry rock using the Munsell color chart. The heading percent vesicle (% Ve) refers only to round cavities (that were presumed to be gas filled) and does not refer to irregular vugs and voids of unknown origin. Percent oxide minerals (% Ox) and percent sulfide minerals (% S) are estimates based on the abundance of grains greater than 50 μm observed in hand specimen with the binocular microscope.

3. The Igneous Mineralogy Log (Appendix C) includes the core, section, pieces, and cm interval of each unit as given in the Igneous Lithology Log. For each unit the abundance, average grain size, and morphology of each mineral phase were recorded. Abundance and size were determined for both phenocryst and groundmass crystals. A hyphen (-) is entered to indicate the absence of a phase. If the rock contains a mineral as phenocrysts and in the groundmass, the morphology of the phenocrysts is reported first, and the groundmass second. Textural term abbreviations are given in Table 2. The rock name for each unit was derived from the mineralogy using the criteria described in the "Rock Names" section of this chapter, and was recorded on both the Igneous Contacts and the Igneous Lithology Logs.

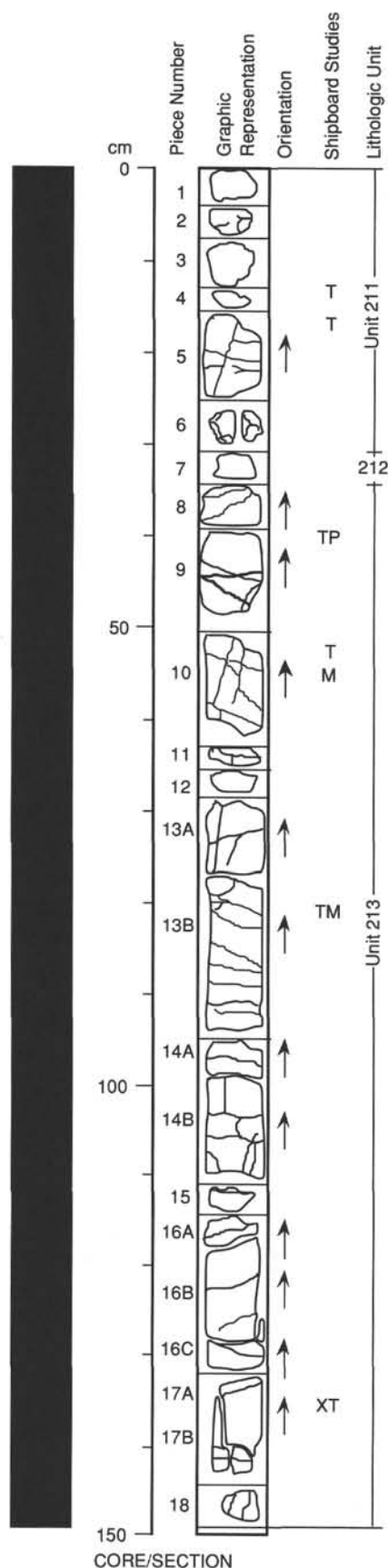
Table 1. Rock textures.

Rock texture			
I.	Porphyritic		
	a. Trachytic	d. Vesicular	g. Protoclastic
	b. Laminated	e. Diktytaxitic	h. Cataclastic
	c. Lineated	f. Myrolitic	i. Foliated
II.	Seriate porphyritic		
III.	Glomeroporphyritic		
IV.	Orthocumulate		
V.	Mesocumulate		
VI.	Adcumulate		
VII.	Aphanitic—microcrystalline		
VIII.	Aphanitic—cryptocrystalline		
IX.	Aphanitic—glassy		
X.	Phaneritic—coarse grained		
XI.	Phaneritic—medium grained		
XII.	Phaneritic—fine grained		
XIII.	Completely altered, no texture determined		
XIV.	Poikilitic		
XV.	Doleritic		
XVI.	Equigranular		

Thin sections of igneous rocks were examined to complement and refine the hand-specimen observations. The abundance of each mineral phase was determined by counting 500 points using an automatically advancing stage with an attached counter. Two separate point counts were made: one by an igneous petrologist counting primary mineral abundances (alteration is ignored if the original mineral phase can be identified), and a second by a metamorphic petrologist counting the actual abundances of unaltered minerals and

³ For further information, consult Engineering and Drilling Operations, Ocean Drilling Program, 1000 Discovery Drive, College Station, TX 77845-9547, U.S.A.

140-504B-186R-1

**UNIT 211: MODERATELY PLAGIOCLASE-CLINOPYROXENE-OLIVINE PHYRIC DIABASE****Pieces 1-6****CONTACTS:** Not observed.**PHENOCRYSTS:**

Plagioclase - 3.0%; 3.0 mm; euhedral.

Augite - 0.5%; 0.8 mm; subhedral.

Olivine - 0.3%; 2.5 mm; euhedral.

Cr-Augite - 2.0%; 6.5 mm; euhedral.

GROUNDMASS: Texture: Fine-grained doleritic. Composition: Plagioclase, clinopyroxene, Fe-Ti oxide minerals.**VESICLES:** Non-vesicular.**COLOR:** Bluish gray (5B 5/1).**STRUCTURE:** Massive.**ALTERATION:** Slightly altered. Olivine: 100% altered to chlorite, actinolite, pyrite, chalcopyrite, and iron oxide minerals. Groundmass: 10% altered to actinolite, chlorite, albite, and titanite.**VEINS/FRACTURES:** <0.5-1 mm; unoriented. Five open fractures, 1 dark green vein, 1 light green vein.**ADDITIONAL COMMENTS:** Sulfide associated with altered olivine. Gabbroic xenoliths in Pieces 4 and 5. Two types of cumulate gabbroic xenoliths: (1) olivine-bearing plagioclase+clinopyroxene ± Fe-Ti oxide minerals, and (2) olivine-free plagioclase+clinopyroxene (without visible Fe-Ti oxide minerals). Composite pyroxenite-gabbro nodule in Piece 2.**UNIT 212: APHYRIC DIABASE****Piece 7****CONTACTS:** Not observed.**PHENOCRYSTS:**

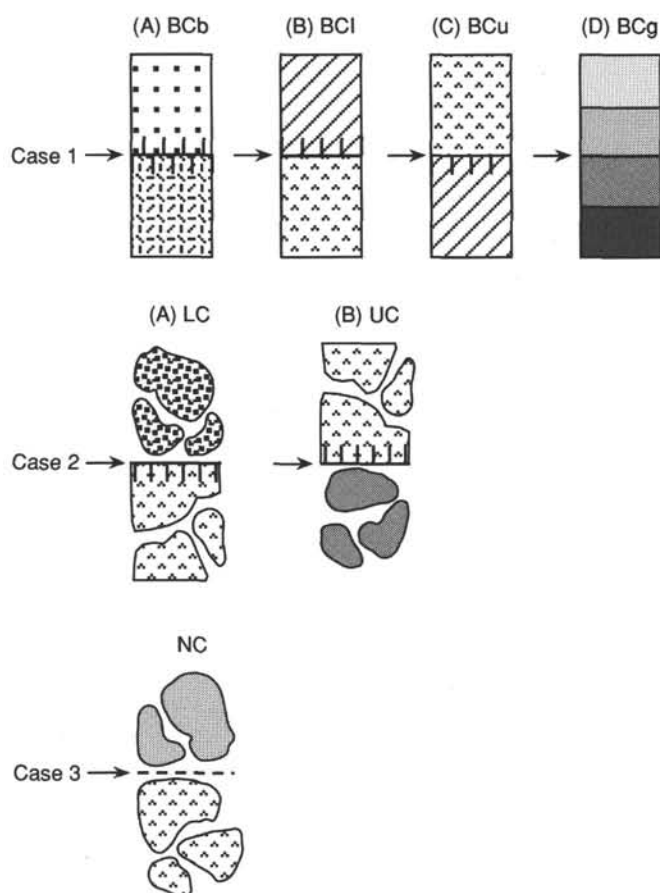
Plagioclase - 0.2%; 2.5 mm; euhedral.

Augite - 0.2%; 0.8 mm; subhedral.

Cr-Augite - 0.2%; 6.5 mm; euhedral.

GROUNDMASS: Texture: Fine-grained, equigranular. Composition: Plagioclase, clinopyroxene, Fe-Ti oxide minerals.**VESICLES:** Non-vesicular.**COLOR:** Bluish gray (5B 5/1).**STRUCTURE:** Massive.**ALTERATION:** Slightly altered. Olivine: 100% altered to chlorite, actinolite, pyrite, chalcopyrite, serpentine, and magnetite. Groundmass: 10% altered to actinolite, chlorite, albite, and titanite.**VEINS/FRACTURES:** No fractures or veins.

Figure 4. Visual core description form (VCD).

**Case 1**

Contact between two units recovered

- (A) BCbchilled margins on both sides
 (B) BClchilled against the lower unit
 (C) BCuchilled against the upper unit
 (D) BCggradational

Case 2

Contact between two units not recovered

- (A) LCupper boundary of the lower unit obtained
 (B) UClower boundary of the upper unit obtained

Case 3

NCcontact between two units not recovered;
 both boundaries unknown

Table 2. Individual mineral morphologies.

Individual mineral morphologies

- | | | |
|--|---------------------------|--------------------|
| 1. Phenocryst | f. Exsolution | k. Partly resorbed |
| a. Anhedral | g. Fluid inclusions | l. Skeletal |
| b. Subhedral | h. Melt inclusions | m. Pseudomorph |
| c. Euhedral | i. Mineral inclusions | |
| d. Zoned | j. Reaction rim or corona | |
| e. Twinned | | |
| 2. Microphenocryst | | |
| 3. Subophitic crystal | | |
| 4. Ophitic crystal | | |
| 5. Oikocryst | | |
| 6. Chadacryst | | |
| 7. Cumulus crystal | | |
| 8. Intercumulus crystal | | |
| 9. Crescumulus crystal | | |
| 10. Discrete crystal laths in diabasic texture | | |

HARVI Database

The Igneous Contacts, Lithology, and Mineralogy Logs are presented as appendices, and summary descriptions of each rock unit are available from the computerized database at ODP. To ensure consistency with previous studies, data from the igneous logs were entered into the HARVI computerized database. The database is divided into separate data sets for fine-grained rocks and coarse-grained rocks. Each record is checked by the database program for consistency and completeness, and is subsequently printed in a format that can be directly pasted onto the barrel sheet for curatorial handling. For each lithologic unit and section, the following information was recorded in the HARVI database system:

- A. the leg, site, hole, core number, core type, and section number;
- B. the unit number (consecutive downhole), position in the section, number of pieces of the same lithologic type, the rock name, and the identification of the observer;
- C. the Munsell color number of the dry rock and the presence and character of any structural fabric;
- D. the number of mineral phases visible with a hand lens and their distribution within the unit, together with the following information for each phase: (1) abundance (volume %); (2) size range in mm; (3) shape (anhedral, subhedral, or euhedral); (4) degree of alteration; and (5) further comments if appropriate;
- E. the groundmass texture: glassy, fine-grained (<1 mm), medium-grained (1–5 mm), or coarse-grained (>5 mm), (grain-size changes within units were also noted);
- F. the presence and characteristics of secondary minerals and alteration products;
- G. the abundance, distribution, size, shape, and infilling material of vesicles (including the proportion of vesicles that are filled by alteration minerals);
- H. the rock structure: determining whether the unit is massive, pillowed, thin, or sheetlike, brecciated, or a hyaloclastite;
- I. the relative amount of rock alteration, expressed both in the description and next to the graphic description of the archive half;
- J. the presence of veins and fractures, including their abundance, width, mineral fillings or coatings, and orientation;
- K. other comments, including notes on the continuity of the unit within the core and on the interrelationship of units.

Rock Names

Igneous rocks within oceanic crust can be divided into four main categories: extrusive, hypabyssal, plutonic, and ultramafic. In general, fine- to medium-grained rocks that occur in flows, pillows, dikes, or shallow intrusions (extrusive and hypabyssal rocks) are classified using one scheme, and medium- to coarse-grained rocks that occur in deeper

alteration phases. Some of the rocks examined in thin section were seriate porphyritic, a texture in which there is a complete gradation from groundmass to phenocryst morphology for plagioclase and augite. As a result, for some of the samples, phenocrysts and groundmass minerals were not separated in the point counts. In addition to abundances, mineral morphologies, average grain sizes, and textural features were described. Descriptions of mineral inclusions, "xenocrysts" and "xenoliths," and the zoning within minerals were included in the comment section of the Thin-Section Description Form. This information was recorded in the computerized database HRTHIN. The same terminology used for thin-section descriptions was used for the megascopic descriptions (see Tables 1 and 2). Thin-section descriptions are included in the appendices and are also available from the ODP computerized database.

Figure 5. Types of igneous contacts observed in drill core.

intrusions or as residual crystals (plutonic and ultramafic rocks) are classified using another. The division between these two classification schemes is somewhat arbitrary. Fine-grained rocks are considered to have an average grain size of 1 mm or less, medium-grained rocks have an average grain size between 1 mm and 5 mm, and coarse-grained rocks have an average grain size of more than 5 mm.

Fine- to medium-grained rocks are termed aphyric (<1%), sparsely phytic (1%–2%), moderately phytic (2%–10%), or highly phytic (>10%), depending upon the proportion of megacrysts or phenocrysts visible with the hand lens or binocular microscope, and are further classified by the types of phenocrysts or megascopic crystals present (e.g., moderately plagioclase-olivine phytic). Similar abbreviations for these rock names have been adopted as in Legs 69, 70, 83, 111, and 137: P, O, C, OP, OPC, and A where P = plagioclase, O = olivine, C = clinopyroxene, and A = aphyric; on Leg 140, however, phenocryst phases were listed in order of abundance adding the additional categories: PO, OC, CP, POC, OCB, COP, and CPO. Rocks with significant amounts or distinctive types of metamorphic minerals or textures may also be given metamorphic modifiers (e.g., cataclastic diabase). Previous legs at Hole 504B have used the root word “basalt” to describe both extrusive and hypabyssal intrusive rocks of basaltic composition. The majority of the rocks recovered on Leg 140 are holocrystalline, fine- to medium-grained rocks with doleritic textures, and the root word “diabase” has been used for these rocks. The few samples recovered which contain glass or devitrified glass were given the root word “basalt.” These basalt samples probably include both chilled dike margins and samples of pillow lava from higher up in the section which fell into the hole and were sampled by subsequent coring.

Whenever possible plutonic and ultramafic rocks are classified according to their primary mineralogy (see Figs. 6, 7, 8, 9). Mineral modifiers are added to plutonic and ultramafic rock names to denote abundant or unusual accessory minerals (e.g., ilmenite-gabbro or phlogopite-dunite) or to include unusual textural features (e.g., miarolitic-gabbro or laminated-dunite). Cumulate rocks have a prefix code to list the cumulate phases (e.g., poaC gabbro for a gabbro with cumulus plagioclase, olivine, and augite, or bimC orthopyroxenite for an orthopyroxenite with cumulus bronzite, ilmenite, and magnetite).

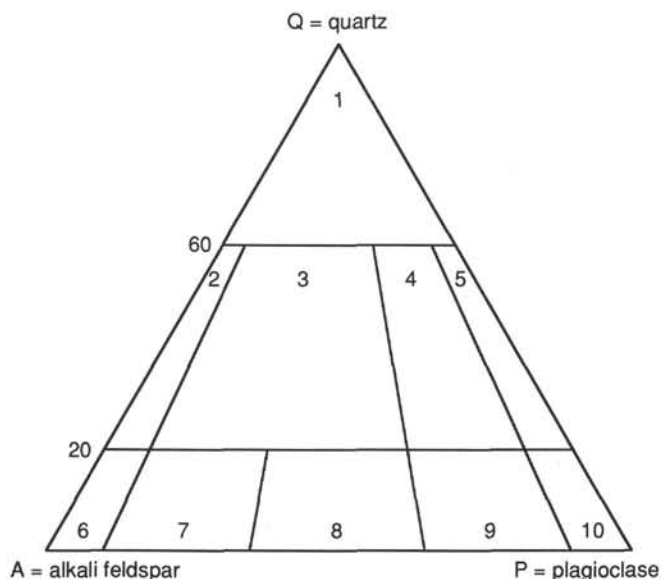


Figure 6. Classification diagram for plutonic rocks with less than 90% total mafic phases. Fields: 1, quartz-rich granitoids; 2, alkali-feldspar granite; 3, granite; 4, granodiorite; 5, tonalite; 6, alkali-feldspar syenite; 7, syenite; 8, monzonite; 9, monzodiorite (plagioclase <An₅₀), or monzogabbro (plagioclase >An₅₀); 10, diorite (plagioclase <An₅₀), gabbro (plagioclase >An₅₀), or anorthosite (total plagioclase >90%). After Streckeisen (1976).

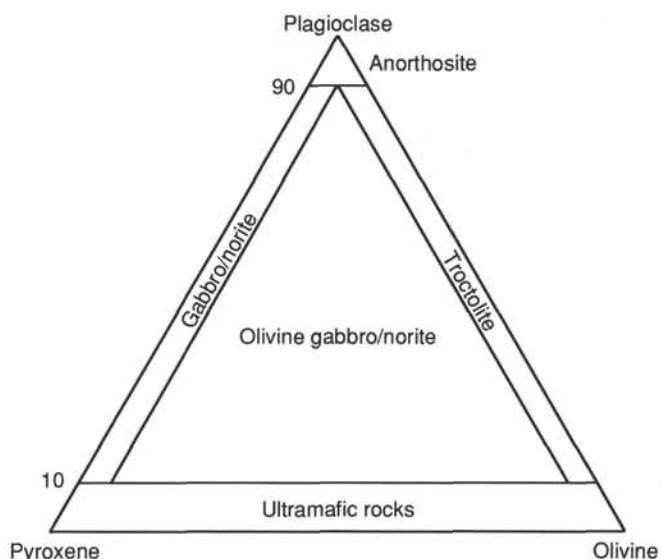


Figure 7. Classification of gabbros composed primarily of plagioclase, pyroxene, and olivine. After Streckeisen (1976).

Rocks with significant amounts or distinctive types of metamorphic minerals or textures may also be given metamorphic modifiers (e.g., serpentinized gabbro). Rocks in which the original mineralogy and texture are no longer discernible are named using the appropriate metamorphic rock classification.

ALTERATION AND METAMORPHISM

Metamorphic and alteration visual core descriptions (see Appendices F, G, H, and I; Appendix G is on microfiche in back pocket) were conducted following igneous documentation of the core. To provide consistent and complete characterization of the core, metamorphic, alteration, and vein visual core description logs, described below, were used and a subset of the data was entered into the computerized database HARVI. In order to ensure accurate core

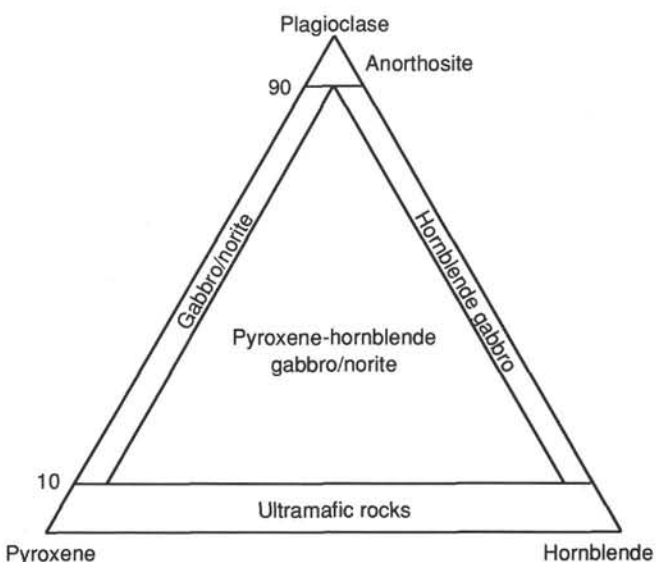


Figure 8. Classification of gabbros composed primarily of plagioclase, pyroxene, and igneous hornblende. After Streckeisen (1976).

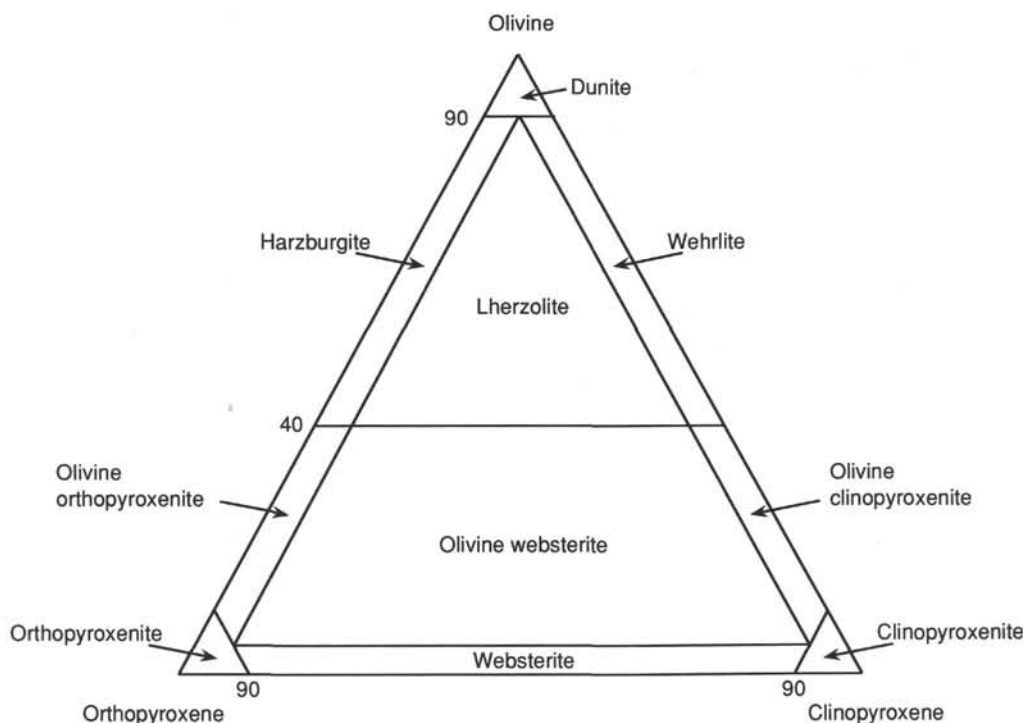


Figure 9. Classification of ultramafic rocks. After Streckeisen (1976).

descriptions, thin-section petrography was integrated with visual core descriptions where possible. The metamorphic, alteration, and vein logs include documentation of core metamorphism, alteration, mineralogy, and petrology, and definition of metamorphic and alteration units. The metamorphic log (Fig. 10) was intended for deformational features and related mineral phases where the rocks are extensively deformed and/or completely recrystallized, but was not used because such rocks were not recovered. The alteration log (Fig. 11), which includes descriptions of secondary features unrelated to deformation such as alteration halos and secondary mineralogy, was used for undeformed rocks in the recovered core where relict igneous minerals and textures were easily recognized.

Abbreviations of lithology, color, and mineralogy that were used in the metamorphic, alteration, and vein logs are listed in Table 3.

When describing sequences of rocks, the core was examined for different metamorphic and alteration units on the basis of changes in secondary mineral occurrence and abundance in both rocks and veins, as well as texture, grain size, rock composition, and presence and type of breccias. Such metamorphic and alteration units could overlap or crosscut

lithologic units defined by igneous features. For each unit and section, the following information was recorded in the log database.

A. The leg, site, hole, core number, core type, section number, piece number (consecutive downhole), and position in the section were recorded in the metamorphic, alteration, and vein log sheets. Lithologies were recorded in the metamorphic and alteration databases.

The following information was recorded in the individual databases.

B. Metamorphic Log: The metamorphic log was intended to describe rock in which the original igneous character was completely obscured by deformation and alteration. Metamorphic units are defined by mineralogy and abundance (volume %) of porphyroblast and neoblast phases, as well as determination of mineral phases and abundance of phases which define the foliation. Characterization of breccias includes clast lithology and secondary mineralogy, matrix mineralogy, and abundance of clasts and mineral phases.

C. Alteration Log: The alteration log was used to describe rocks with a clear igneous progenitor. Alteration mineralogy includes the primary phase being altered, alteration products and secondary mineral phases, and volume percent of each secondary phase. These were estimated in hand specimen and estimates were verified and "calibrated" by thin-section examination. Characterization of amygdules and related alteration halos includes size, percent of host rock alteration, and mineralogy of vug-filling minerals and mineral phases defining the halos.

D. Vein Log: Vein type was based on color and/or mineralogy, width (mm) and orientation, and texture of vein-filling minerals and mineral abundance (Fig. 12). Documentation of vein-related alteration halos includes halo type (based on color), abundance of secondary phases comprising the halo, halo width, and abundance of halos as percentage of halos per piece.

GEOCHEMISTRY

X-ray Fluorescence Analyses

Samples considered by the shipboard party to be representative of individual lithologic units or of unusual composition were analyzed

Table 3. Abbreviations of lithology.

Lithology
Amph'ite = amphibolite; BS = basalt; Mylon = mylonite; DB = diabase; Cata = cataclastite; GB = gabbro; FG = fine-grained gabbro; MG = metagabbro
Color:
bm = brown; gm = green
Mineralogy:
cly = clay minerals; cp = chalcopyrite; cpx = clinopyroxene; ab = albite; ac = actinolite; anl = analcime; an = anorthite; ap = apatite; ba = barite; bi = biotite; cc = calcite; chl = chlorite; cum = cummingtonite; cz = clinozoisite; ep = epidote; FeOx = iron oxide; hb = hornblende; ilm = ilmenite; ksp = K feldspar; ml-clay = mixed layer clay; mt = magnetite; mus = muscovite; ox = oxides; pre = prehnite; py = pyrite; qtz = quartz; rut = rutile; ser = serpentine; sm = smectite; tlc = talc; tre = tremolite; tt = titanite; zeo = zeolite.

Figure 10. Example of metamorphic log form.

Figure 10. Example of metamorphic log form.

Core	Section	Piece	Interval (cm)		Lithology	After olivine	%	After plagioclase	%	After augite	%	After others	%	After groundmass	%	Halo	AW (cm)	%	Amygdules	AD (cm)	%	Comments
173R	1	1-13	0	139	DB	chl.py	100	---	0	---	0	---	0	ac.chl.py cpy.tt	15							Slightly to moderately altered. Amy. are rare w/dark gr act-chl cores and light gray-gr halo of ab.ac.chl.tt.
173R	1	1.2	0	12	DB	chl.py	100	---	0	---	0	---	0	ac.chl.py	15	ab.ac.tt.chl	0.3	10	ac.chl	0.5	3	
173R	1	6.7	54	64	DB	chl.py	100	---	0	---	0	---	0	ac.chl.py cpy.tt	15	ab.ac.tt.chl	0.5	20	ac.chl	0.3	10	Piece 6, 1.5-cm-wide halo + amyg at top of sample.
173R	1	9	72	79	DB	chl.py	100	---	0	---	0	---	0	ac.chl.py cpy.tt	15	ab.ac.tt.chl	0.7	30	ac.chl	0.8	15	Highly alt. due to coalescing amyg. + halo.
173R	1	12.13	116	139	DB	chl.py	100	---	0	---	0	---	0	ac.chl.py cpy.tt	15	ab.ac.tt.chl	0.4	5	ac.chl	0.5	3	Same as Pieces 1 and 2.
173R	2	1-4	0	34	DB	chl.py	100	---	0	---	0	---	0	ac.chl.py cpy.tt	15	---	0.0	0	---	0.0	0	Slightly to moderately altered. Amy. are rare w/dark gr ac-chl cores and light gray-gr halo.
173R	2	2.3	11	27	DB	chl.py	100	---	0	---	0	---	0	ac.chl.py cpy.tt	15	ab.ac.tt.chl	0.3	5	ac.chl	0.4	4	
174R	1	1-22	0	146	DB	chl.py	100	white ab-zeo	20	---	0	---	0	ac.chl.py cpy.tt	15							Slightly altered, locally highly altered due to amyg + halo. Amyg. are rare w/dark gr cores and light gray-gr halo. Dissem. py. Moderately to highly altered due to halo.
174R	1	2.3	6	19	DB	chl.py	100	white ab-zeo	20	---	0	---	0	ac.chl.py cpy.tt	15	ab.ac.tt.chl	0.0	60	ac.chl	0.0	0	
174R	1	5	32	34	DB	chl.py	100	white ab-zeo	20	---	0	---	0	ac.chl.py cpy.tt	15	ab.ac.tt.chl	0.3	5	ac.chl	0.2	2	
174R	1	7-10	43	69	DB	chl.py	100	white ab-zeo	20	---	0	---	0	ac.chl.py cpy.tt	15	ab.ac.tt.chl	0.7	20	ac.chl	0.3	5	Piece 9, moderately altered due to halo, 30-40% diffuse amygdules.
174R	1	13	84	87	DB	chl.py	100	white ab-zeo	20	---	0	---	0	ac.chl.py cpy.tt	15	ab.ac.tt.chl	0.3	3	ac.chl	0.0	0	Very thin halo on edge of sample.
174R	1	16-22	100	146	DB	chl.py	100	white ab-zeo	20	---	0	---	0	ac.chl.py cpy.tt	15	ab.ac.tt.chl	0.3	10	ac.chl	0.5	5	
174R	1	17-18	106	118	DB	chl.py	100	white ab-zeo	20	---	0	---	0	ac.chl.py cpy.tt	15	ab.ac.tt.chl	0.3	10	ac.chl	0.8	10	Piece 17, coalescing halo, moderately altered.
174R	2	1-16	0	100	DB	chl.tlc.py FeOx	100	white ab	10	---	0	---	0	ac.chl.py cp.tt	15							Slightly altered, locally highly altered due to amyg + halo. Amyg. are rare w/dark green cores and light gray-green halo. Dis. py.
174R	2	8.9	41	53	DB	chl.tlc.py FeOx	100	white ab	10	---	0	---	0	ac.chl.py cy.tt	15	ab.ac.tt.chl	0.2	3	act.chl	0.4	2	
174R	2	11-14	60	88	DB	chl.tlc.py FeOx	100	white ab	10	---	0	---	0	ac.chl.py cy.tt	15	ab.ac.tt.chl	0.3	15	act.chl	0.4	3	
175R	1	1-6	0	42	DB	chl.tlc.py	100	---	0	---	0	---	0	ac.chl.py cy.tt	15							Slightly altered. No amyg. Disseminated py.
176R	1	1-24	0	133	DB	chl.tlc.py ml-clay	100	white ab	10	---	0	---	0	ac.chl.py cp.tt	15							Slightly altered, locally highly altered due to amyg + halo. Amyg. are rare w/dark gr cores and light gray-gr halo.
176R	1	5-11	24	63	DB	chl.tlc.py ml-clay	100	white ab	10	---	0	---	0	ac.chl.py cy.tt	50	---	0.1	0	---	0.1	0	Mod to highly altered. No amyg. or halo.
176R	1	12	64	67	DB	chl.tlc.py ml-clay	100	white ab	10	---	0	---	0	ac.chl.py cp.tt	15	ab.ac.tt.chl	0.2	3	act.chl	0.1	0	Diffuse amygdules.
176R	1	14-17	73	93	DB	chl.tlc.py ml-clay	100	white ab	10	---	0	---	0	ac.chl.py cy.tt	15	ab.ac.tt.chl	0.2	5	act.chl	0.4	3	Pieces 15,16, elongate zone of coalescing halo.
176R	1	20-22	106	121	DB	chl.tlc.py ml-clay	100	white ab	10	---	0	---	0	ac.chl.py cy.tt	15	ab.ac.tt.chl	0.2	10	act.chl	0.3	3	
177R	1	1-17	0	74	DB	chl.py ml-clay	100	---	0	---	0	---	0	ac.chl.py cy.tt	15	---	0.1	0	---	0.1	0	Slightly altered. No amygdules. Fine-grained.
178R	1	1-4	0	25	DB	chl,ml-clay ser. ac	100	---	0	---	0	---	0	ac.chl.py cy.tt	15							
178R	1	4	20	25	DB	chl,ml-clay ser, ac	100	---	0	---	0	---	0	ac.chl.py cp.tt	15	ab.ac.tt.chl	0.2	3	act.chl	0.5	4	
180M	1	1-9	0	116	DB	chl,ac.py FeOx,tt,tlc ml-clay	100	---	0	---	0	---	0	ac.chl.py cp.tt	15							Slightly altered, locally highly altered due to amygdules + halo.
180M	1	6	65	66	DB	chl,ac.py FeOx,tt,tlc ml-clay Colorless??	100	---	0	---	0	---	0	ac.chl.py cp.tt	15	ab.ac.tt.chl	0.4	10	act.chl	0.6	2	Halo 80% recrystallized.
180M	1	7-9	76	116	DB	chl,ac.py FeOx,tt,tlc ml-clay Colorless??	100	---	0	---	0	---	0	ac.chl.py cp.tt	15	ab.ac.tt.chl	0.3	15	act.chl	0.2	2	Halo diffuse, elongate, 80% recrystallized.
180M	2	1-8	0	120	DB	chl.py,FeOx	100	---	0	---	0	---	0	ac.chl.py cp.tt	15							Slightly altered, locally highly altered due to amygdules + halo.

Figure 11. Example of alteration log. See Appendix F in "Site 504" chapter (this volume).

Core	Section	Piece	Interval (cm to cm)	Vein type	Vein minerals	α	AW (mm)	Orientation Dip Az	Halo type	Alt %	AW (mm)	α	Comments
173R	1	2	8 10	frac (1)	none	<1	0.5	48 75	none	0	0	0	
173R	1	6	54 59	frac (2)	none	<1	0.5		none	0	0	0	2 discont. fracs.
173R	1	7	60 64	fracs	none	<1	0.5		none	0	0	0	
173R	1	12	116 118	frac (3)	none	<1	0.5	15 164	none	0	0	0	3 fracs.
173R	1	12	121 122	fracs	none	<1	0.5	15 173	none	0	0	0	
173R	1	13	127 139	fracs	none	<1	0.5	13 244	none	0	0	0	
173R	2	2	11 17	fracs	none	<1	0.5		none	0	0	0	Discont., <3 cm long.
173R	2	3	19 25	fracs	none	<1	0.5	82 37	none	0	0	0	
173R	2	3	21 25	frac (2)	none	<1	0.5	7 196	none	0	0	0	2, subhorizontal.
173R	2	4	29 35	dk gm (1)	chl + mt?	<1	0.5		none	0	0	0	Short, irregular.
174R	1	2	7 12	dk gm (1)	chl	1	0.5-1		lt gm	60	4	20	
174R	1	3	17 19	frac (1)	none	<1	0.5	77 245	none	0	0	0	
174R	1	5	32 35	frac (1)	none	<1	0.5		none	0	0	0	
174R	1	7	43 48	frac (1)	none	<1	0.5	81 260	none	0	0	0	
174R	1	8	50 57	frac (1)	none	<1	0.5	78 128	none	0	0	0	3 fracs.
174R	1	8	50 57	frac (1)	none	<1	0.5	74 213	none	0	0	0	
174R	1	9	58 59	dk gm (1)	chl	1	0.5		lt gm	60	5	15	
174R	1	9	60 61	dk/lt gm	chl + ac	1	0.5		lt gm	60	5	15	
174R	1	9	58 59	lt gm	ac + pl?	1	0.5		none	0	0	0	
174R	1	10	64 69	frac (2)	none	1	0.5		none	0	0	0	2 fracs.
174R	1	13	83 87	frac (1)	none	<1	0.5		none	0	0	0	
174R	1	15	94 96	frac (1)	none	<1	0.5	37 231	none	0	0	0	
174R	1	17	108 110	frac (1)	none	<1	0.5	31 218	none	0	0	0	
174R	1	18	117 118	frac (1)	none	<1	0.5	4 90	none	0	0	0	
174R	1	18	115 116	frac (1)	none	<1	0.5		none	0	0	0	
174R	1	20	129 133	frac (1)	none	<1	0.5		none	0	0	0	
174R	1	22	142 146	frac (1)	none	<1	0.5		none	0	0	0	
174R	2	1	0 3	dk/lt gm (1)	chl + ac	<1	<0.5		lt gm	60	3	20	
174R	2	2	7 8	frac (1)	none	<1	0.5		none	0	0	0	Discont.
174R	2	5	23 27	frac (1)	none	<1	0.5		none	0	0	0	Discont.
174R	2	7	33 35	frac (4)	none	<1	0.5	38 262	none	0	0	0	4 fracs.
174R	2	7	36 37	frac (1)	none	<1	0.5	29 270	none	0	0	0	
174R	2	8	42 44	frac (4)	none	<1	0.5	14 94	none	0	0	0	4-5 fracs, radiate from one point.
174R	2	8	42 46	frac (1)	none	<1	0.5	38 307	none	0	0	0	
174R	2	9	49 53	frac (1)	none	<1	0.5		none	0	0	0	
174R	2	13	76 80	frac (3)	none	<1	0.5		none	0	0	0	3 fracs.
174R	2	14	82 83	frac (1)	none	<1	0.5	27 8	none	0	0	0	
174R	2	14	85 86	frac (1)	none	<1	0.5	9 221	none	0	0	0	
174R	2	15	89 92	frac (1)	none	<1	0.5		none	0	0	0	
174R	2	16	94 100	frac (3)	none	<1	0.5		none	0	0	0	3 fracs.
175R	1	3A	19 20	dk gm (1)	chl	<1	0.5	55 0	lt gm	60	2	tr	Rock broken along this and next, conjugate veins.
175R	1	3A	17 20	dk gm (1)	chl	<1	0.5	67 112	lt gm	60	1	tr	See structural sketch.
175R	1	3A	11 12	frac (1)	none	<1	<0.5	21 111	none	0	0	0	
175R	1	3A	14 15	frac (1)	none	<1	<0.5	10 143	none	0	0	0	
175R	1	3B	20 21	frac (1)	none	<1	<0.5	14 348	none	0	0	0	
175R	1	5	34 35	frac (1)	none	<1	<0.5	5 101	none	0	0	0	
175R	1	5	35 36	frac (1)	none	<1	<0.5	1 135	none	0	0	0	
175R	1	6	38 42	frac (1)	none	<1	<0.5		none	0	0	0	
176R	1	3	15 19	dk gm (1)	chl	1	0.5		lt gm	60	3	10	
176R	1	5	24 28	wht/gm (1)	lau + chl	nd	nd		none	0	0	0	Disaggregated, crystals to 1 cm long, acicular.
176R	1	6	29 32	wht/gm (1)	lau + chl	nd	nd		none	0	0	0	Lau attached to rock frag surfaces.
176R	1	7	33 40	wht/gm (1)	lau + chl	nd	nd		none	0	0	0	Ditto.
176R	1	8	41 49	wht/gm (1)	lau + chl	nd	nd		none	0	0	0	Ditto.
176R	1	10	54 57	wht/gm (1)	lau + chl	nd	nd		none	0	0	0	Ditto.
176R	1	10	54 57	dk gm (1)	chl	1	1		none	0	0	0	Irregular, branching.
176R	1	11	58 63	dk gm (1)	chl	2	0.5		lt gm	60	3	20	
176R	1	12	64 67	dk gm (1)	chl	<1	<0.5		none	0	0	0	Very small.
176R	1	14	72 77	frac (1)	none	<1	<0.5		none	0	0	0	
176R	1	15	78 84	frac (1)	none	<1	<0.5		none	0	0	0	

Figure 12. Example of vein log. See Appendix G (back pocket) in "Site 504" chapter (this volume).

for major and selected trace elements by X-ray fluorescence (XRF). The on-board XRF system (Applied Research Laboratory 8420) is a fully automated, wavelength-dispersive spectrometer employing a 3-kW rhodium target X-ray tube as the excitation source for both major and trace elements. The current list of analyzed elements and operating conditions is presented in Table 4. Except for minor changes in counting times for several elements (Mg, K, Ti, Zn, Cu, Ni, Cr, V), these parameters have remained unchanged since Leg 111. All samples for major element analysis were prepared and measured in duplicate. Trace element samples were prepared as single pellets, but each was measured twice. Estimates of precision and lower limits of detection are presented in the site chapter (this volume, table 7).

Crushing and Grinding

Following cutting by either water-cooled saws or 1-in. diameter diamond drill cores, samples were wet-ground on diamond abrasive wheels to remove saw marks or any unwanted material. The average sample taken weighed approximately 22 g. For estimating sampling errors due to sample size (e.g., Clanton and Fletcher, 1976), the weight of each sample was recorded along with the analyses in Table 4. After grinding, the samples were sonicated in distilled water and methanol for 10 min each, followed by drying at 110°C for at least 2 hr. Larger

pieces were reduced to less than 1-cm diameter by crushing samples between two disks of Delrin plastic in a hydraulic press. Finally, powders were produced by grinding in a tungsten carbide shatterbox vessel for approximately 1–2 min. Sample contamination from the tungsten carbide shatterbox is significant for elements W, Co, and Ta (Thompson and Bankston, 1970). At these grinding times, however, niobium contamination is minimal (<1 ppm).

Major Elements

Major elements were determined on fused glass discs in order to reduce matrix influences and eliminate particle size effects (Norris and Hutton, 1969). Prior to fusion, fresh rock powders were ignited at 1,000°C for 4 hr. This represents a doubling of the ignition time from previous legs, but was chosen to ensure complete dehydration of all hydrous mineral phases expected from Hole 504B samples, particularly amphibole. The discs were then prepared by mixing 6.00 g of lanthanum-doped lithium tetraborate flux (Spex #FF28-10) with 0.500 g of ignited rock powder, followed by fusion in platinum-gold (Pt₉₅Au₅) crucibles at 1030°C for approximately 8 min. The molten sample/flux mixture was then poured into Pt₉₅Au₅ molds and cooled using a modified Claisse Fluxer apparatus. Because the powders were ignited prior to weighing, all analyses are reported on an anhydrous

Table 4. X-ray spectrograph analytical conditions.

Oxide or element	Line	Crystal	Detector	Collimator angle	Peak offset	Background	Count time (degrees 2θ) on peak(s)	Count time (degrees 2θ) on background(s)
SiO ₂	K-alpha	PET	FPC	Coarse	109.25	±0.00	40	0
TiO ₂	K-alpha	LiF(200)	FPC	Coarse	86.14	±0.00	100	0
Al ₂ O ₃	K-alpha	PET	FPC	Coarse	145.27	±0.00	100	0
Fe ₂ O ₃ *	K-alpha	LiF(200)	FPC	Fine	57.52	±0.00	40	0
MnO	K-alpha	LiF(200)	KrSC	Fine	62.98	±0.00	40	0
MgO	K-alpha	TLAP	FPC	Coarse	44.87	±0.80	200	200
CaO	K-alpha	LiF(200)	FPC	Coarse	113.16	±0.00	40	0
Na ₂ O	K-alpha	TLAP	FPC	Coarse	54.71	-1.20	200	200
K ₂ O	K-alpha	LiF(200)	FPC	Coarse	136.65	±0.00	100	0
P ₂ O ₅	K-alpha	Ge(111)	FPC	Coarse	140.94	±0.00	100	0
Rh	K-alpha Compton	LiF(200)	Scint	Fine	18.563	±0.00	60	0
Nb	K-alpha	LiF(200)	Scint	Fine	21.359	±0.35	200	200
Zr	K-alpha	LiF(200)	Scint	Fine	22.514	±0.35	100	100
Y	K-alpha	LiF(200)	Scint	Fine	23.756	±0.40	100	100
Sr	K-alpha	LiF(200)	Scint	Fine	25.106	±0.41	100	100
Rb	K-alpha	LiF(200)	Scint	Fine	26.574	±0.60	100	100
Zn	K-alpha	LiF(200)	Scint	Coarse	41.759	±0.55	100	100
Cu	K-alpha	LiF(200)	Scint	Coarse	44.985	±0.55	100	100
Ni	K-alpha	LiF(200)	Scint	Coarse	48.617	±0.60	100	100
Cr	K-alpha	LiF(220)	FPC	Fine	69.356	±0.50	100	100
Fe	K-alpha	LiF(200)	FPC	Fine	85.701	±0.70	40	40
V	K-alpha	LiF(200)	FPC	Fine	123.173	-0.50	100	100
Ti	K-alpha	LiF(220)	FPC	Fine	86.153	±0.50	40	40

basis, and all iron values are reported as total iron as Fe₂O₃ (listed as Fe₂O₃*).

The 12:1 flux-to-sample ratio reduces matrix influences to the point where matrix corrections are usually unnecessary for normal basaltic to granitic compositional ranges. Therefore, simple linear relationships exist between X-ray intensities and oxide concentrations, so that concentrations can be expressed as

$$C_i = (I_i \times m_i) - b_i$$

Where C_i = concentration (wt%) of oxide i

I_i = net peak intensity (counts/s) of oxide i

m_i = calibration factor (wt%/counts/s) of oxide i

b_i = measured blank (wt%) of oxide i .

The calibration factor (m_i) is determined by measuring natural and synthetic standards. Table 5 lists the analyses of these standards obtained after major element calibrations on Leg 140. When extreme compositions such as MgO in ultramafic rocks or CaO in calcareous sediments are to be analyzed, standards closer in composition to the unknowns should be used. For more details on calibrating major elements, see the Leg 111 "XRF Analyses" section in the "Introduction and Explanatory Notes" chapter (Becker, Sakai, et al., 1988, p. 9-10).

Trace Elements

Trace elements were determined on pressed-powder pellets made by mixing 7 g of fresh rock powder with 30 drops of polyvinyl alcohol

Table 5. Major element analyses of rock and mineral reference standards following Leg 140 calibration.

Standard	Sample type	SiO ₂	TiO ₂	Al ₂ O ₃	Fe ₂ O ₃ *	MnO	MgO	CaO	Na ₂ O	K ₂ O	P ₂ O ₅
AGV-1	Andesite	60.18	1.07	17.42	6.95	0.10	1.34	4.95	4.28	2.98	0.76
AII-92-29-1	Basalt	49.86	1.74	15.46	10.91	0.17	7.25	10.97	3.06	0.16	0.48
BAS-111	Basalt	49.80	0.78	16.50	9.15	0.15	8.35	13.28	1.82	0.00	0.07
BE-N	Basalt	39.50	2.68	10.14	13.11	0.20	13.64	14.33	3.25	1.45	1.23
BHVO-1	Basalt	49.63	2.71	13.42	12.26	0.17	7.05	11.28	2.28	0.52	0.55
BIR-1	Basalt	47.47	0.94	15.43	11.42	0.17	9.57	13.25	1.86	0.02	0.35
BR	Basalt	39.69	2.72	10.22	13.35	0.21	13.88	14.06	3.08	1.45	1.23
DR-N	Diorite	53.96	1.08	17.82	9.79	0.22	4.23	7.08	2.95	1.75	0.53
G-2	Granite	69.56	0.49	15.52	2.62	0.03	0.73	1.92	4.08	4.53	0.45
GH	Granite	76.55	0.08	-0.03	1.36	0.05	0.00	0.72	3.94	-0.11	0.35
JB-1a	Basalt	53.03	1.29	14.58	9.16	0.15	7.77	9.37	2.79	1.42	0.61
JB-2	Basalt	52.72	1.15	14.62	14.28	0.22	4.35	9.75	2.08	0.41	0.42
JB-3	Basalt	50.72	1.42	17.29	11.88	0.18	4.96	9.72	2.76	0.77	0.57
JGb-1	Gabbro	44.22	1.59	17.79	15.21	0.19	7.86	11.98	1.25	0.23	0.38
JP-1	Peridotite	43.22	0.02	0.83	8.61	0.12	50.05	0.59	0.07	0.00	0.36
MRG-1	Gabbro	39.45	3.79	8.46	17.91	0.17	13.60	14.92	0.73	0.18	0.40
NBS-688	Basalt	47.82	1.15	17.28	10.28	0.16	8.41	12.15	2.10	0.18	0.44
RGM-1	Rhyolite	73.30	0.27	-0.03	1.76	0.04	0.28	1.19	4.04	4.31	0.38
STM-1	Syenite	60.12	0.14	18.64	5.28	0.23	0.05	1.15	9.13	4.33	0.49
UB-N	Serpentine	44.55	0.13	3.30	9.58	0.14	43.61	1.40	0.14	0.01	0.35

Note: Most standards were prepared and analyzed in triplicate, the remaining were measured as duplicates. Values are reported in wt%. Ultramafic standards with MgO values over 30 wt% (JP-1 and UB-N) are roughly 9 relative % higher than their preferred values, and therefore, require a slightly different calibration. Fe₂O₃* is total iron expressed as Fe₂O₃.

binder, and pressing the mixture into an aluminum cap with 7 tons of pressure. A minimum of 5 g for basalt, or 7 g of granite, ensures the sample will be infinitely thick for Rh K-series radiation (20 keV).

Trace element concentrations based on calculation routines modified from Norrish and Chappell (1967), Reynolds (1963, 1967), and Walker (1973) are computed using the following relationship:

$$C_i = (I_i \times A_i) / m_i$$

Where C_i = concentration (ppm) of element i

I_i = net peak intensity (counts/s) of element i , corrected for non-linear background and spectral interferences

A_i = mass absorption coefficient for element i

m_i = calibration factor (ppm/counts/s) of element i .

The calibration factor (m_i) for each element is determined on a wide range of rock and mineral standards. Analyses of these standards obtained during the calibration are given in Table 6. See the Leg 111 "XRF Analyses" section in the "Introduction and Explanatory Notes" chapter (Becker, Sakai, et al., 1988, p. 9–10) for more details of the off-line computer program used for these calculations.

thermally releasing H_2O . Following gas-chromatographic separation of the gases, CO_2 and H_2O^+ were quantitatively determined using a thermal conductivity detector. The bias factor (K) of the CHNS-analyzer was calculated by measuring CCRMP reference gabbro, MRG-1 ($CO_2 = 1$ wt%; $H_2O^+ = 0.98$ wt%).

Analyzed samples were typically splits taken from powders prepared for XRF analysis. Two replicate measurements were performed on each sample. Accuracy was checked with five international reference rocks (Table 7). Reproducibility was tested by analyzing the shipboard basalt sample AII92-29-1 (Staudigel, 1979). The relative standard deviation of 17 replicate analyses was about 9% for both CO_2 and H_2O^+ .

STRUCTURE AND DEFORMATION

Introduction

The structural geology of the core recovered from Hole 504B on Leg 140 is crucial to our understanding of oceanic spreading centers and of the igneous and metamorphic processes active in the genesis of the lower crustal sequence in particular. Specialist structural studies have yet to become standard procedure on Ocean Drilling Program

Table 6. Trace element analyses (in ppm) of rock and mineral reference standards following Leg 140 calibration.

Standard	Type	Nb	Zr	Y	Sr	Rb	Zn	Cu	Ni	Cr	V
AGV-1	Andesite	13.7	235	17.1	633	64.5	101	57	15	3	109
AII92-29-1	Basalt	2.6	128	37.4	128	1.1	90	64	99	243	294
BAS-111	Basalt	0.6	40	20.6	61	0.2	59	92	130	366	246
BE-N	Basalt	112.9	287	27.9	1363	46.8	126	74	279	373	240
BHVO-1	Basalt	19.0	180	26.0	393	9.2	112	136	122	291	309
BIR-1	Basalt	0.2	15	15.1	109	0.6	69	128	160	383	298
BR	Basalt	110.6	284	28.1	1340	46.4	163	74	270	338	243
DR-N	Diorite	7.2	129	24.7	388	71.3	179	49	15	26	215
G-2	Granite	11.6	325	8.3	480	169.3	90	12	4	-1	42
GBM-1	Garnet	1.5	93	30.6	9	0.8	58	28	25	17	49
GH	Granite	93.4	156	75.0	9	381.7	59	5	4	-6	0
MAG-1	Marine mud	15.4	130	23.9	135	147.5	139	30	52	98	139
MRG-1	Gabbro	23.4	110	12.3	270	7.1	213	128	193	528	580
NBS-688	Basalt	4.1	57	19.2	166	1.8	68	93	137	286	225
NIM-D	Dunite	0.0	3	-0.2	3	0.1	91	13	2064	2901	40
PCC-1	Peridotite	0.0	0	-0.1	1	0.1	41	9	2452	2497	37
PG-721	Feldspar	0.1	0	0.0	790	1.1	-4	5	0	3	3
RGM-1	Rhyolite	9.1	240	22.7	102	149.3	31	12	5	3	9
STM-1	Syenite	271.3	1361	44.1	695	115.0	262	1	4	-8	0
UB-N	Serpentine	0.1	4	2.1	7	3.3	88	23	1992	2383	64

Preparation of Inter-laboratory Geochemical Standard

To facilitate future comparisons between geochemical data generated at the many different laboratories participating in research related to Leg 140, an inter-laboratory geochemical standard was prepared from approximately 1 kg of diabase (Sample 137-504B-182M-3, 7–20 cm), following the procedures outlined above. After grinding, accumulated batches of rock powder were homogenized in a 1-gal Ziploc freezer bag for about 1 hr, and then distributed in roughly 30 g aliquots to interested members of the shipboard party. Analytical results from the participating labs will be reported in the Leg 140 *Scientific Results* volume. Shipboard X-ray fluorescence analysis of this standard is presented in the site chapter (this volume, table 8).

Carbon and Water Analyses

Total carbon, as CO_2 , and structural water (H_2O^+) were determined using a Carlo Erba NA 1500 CHNS analyzer. Nitrogen and sulfur concentrations in the investigated rocks were usually below the detection limit of the CHNS analyzer. Fifty to 80 mg of dried (110°C) bulk rock samples were combusted at 1010°C under an oxygen atmosphere, converting organic and inorganic carbon into CO_2 and

legs. Occasional exceptions have been noted, e.g., Leg 131 (Nankai Trough), during which specific objectives that could potentially be addressed by structural studies had been identified from the outset. Leg 140 was one of the first occasions on which an attempt was made to undertake a systematic and integrated approach to the study of tectonic features in an ODP basement borehole.

This section deals with the visual and microscopic core descriptions made on board by the structural geologists. The intention of these records is to identify and describe in as systematic and quantitative way as possible all the structural information present in the core, and in particular to record its orientation.

Macroscopic Core Description

All material, from both working and archive halves, was examined, although measurements were largely made on the working half. Initial data are recorded on a working structural log (Fig. 13) for discrete features, and a deformation log (Fig. 14) for ductile fabrics; data recorded on these logs were later entered into separate spreadsheets (Fig. 15). These were modified during the course of the leg. Detailed, additional observations and sketches are recorded on separate sheets as shown in Figure 16. The most pertinent observations

Table 7. CO₂ and H₂O⁺ values of international and shipboard reference rock standards.

	BHVO-1		JA-1		JB-1a		JG-1a	
	%CO ₂	%H ₂ O ⁺	%CO ₂	%H ₂ O ⁺	%CO ₂	%H ₂ O ⁺	%CO ₂	%H ₂ O ⁺
Analyzed mean	0.05	0.25	0.11	1.05	0.14	1.67	0.11	0.66
1σ	0.01	0.01	0.01	0.10	0.00	0.18	0.01	0.09
Preferred values	0.04	0.16–0.20	n.d.	0.65–0.80	0.18	0.7–1.0	0.07	0.46–0.58

	SY-2		AII-92-29-1	
	%CO ₂	%H ₂ O ⁺	%CO ₂	%H ₂ O ⁺
Analyzed mean	0.49	0.55	0.07	0.91
1σ	0.01	0.05	0.01	0.08
Preferred values	0.46	0.45–0.58	0.5–1.1	

Note: Reference values from Gladney and Roelandts (1988a, b) and Terashima and Ando (1987).

are included in the text, and copies of the original Hand Specimen Descriptions can be obtained from the ODP database. In addition, each particular type of structural observation was made by the same individual throughout the leg, to ensure consistency of observation throughout the recovered section. The following sections are largely an explanation of the structure and deformation logs, because they provide a summary of the procedures used as well as insights into the difficulties and constraints encountered when dealing with structures observed only in core.

Structural Core Description Log

A definition of the various fields in the structural core description form is given in Table 8. The location of a structure was recorded in centimeters from the top of the section, according to conventional ODP procedure. Where a structure extended over an interval, the locations of the top and bottom of its range on the cut face of the core were recorded. The sense of fault displacement was also recorded where the direction of motion (from mylonite lineations or slicken-sides) could be determined.

In an attempt to achieve consistency of nomenclature, the structural geologists agreed on a working descriptive terminology for macroscopic features. This does not imply that these features fall into distinct pigeonholes—there is clearly some gradation and even overlap—but these aspects were brought out by adding modifiers, descriptive comments, and sketches.

Several problems are inherent in any study of this nature. From the point of view of identification of tectonic features, commonly only part of the sampled interval in any one core is actually recovered. This leads to a sampling bias that for structural purposes is particularly acute: material from fault zones in particular may be missing when recovery is less than 100%. When faulted or fractured rock from such zones is recovered, it is often highly disturbed relative to its original position.

Determining the orientation of observed structures is also problematic. Features must initially be oriented relative to local reference coordinates, i.e., the core barrel reference frame, and subsequently corrected to true north and true vertical. The drilling process causes fracturing and rotation of core, such that relative rotations in any individual section or core barrel have occurred, and corrections back to true north may be different for each piece of core. Furthermore, the reference line for each piece is drawn arbitrarily, following visual inspection by the structural geologists, so this temporary reference orientation may potentially be consistent over only a few tens of centimeters.

Measurement of Structures

Measurement of planar features traversing the core at oblique angles can be made in several ways. The convention we employed is that adopted during Leg 135 (Fig. 17) which itself was adapted from that used during Legs 131 and 134. We used a simplified version of the protractor-based instrument described in the Leg 131 *Initial Reports*. The plane normal to the axis of the borehole is referred to as the apparent horizontal plane. On this plane a 360° net is used with a pseudo-north (000°) at the bottom line of the working half of the core, the same convention as that used for shipboard paleomagnetic studies. The face of the split core therefore lies in a plane striking 090°–270°, and dips vertically. An apparent dip can be measured on this surface, and its sense (whether toward 090° or 270°) indicated. If the way the fracture, vein, etc., lies relative to the cut is convenient, the dip and dip direction can be measured directly; otherwise, measurement of one further apparent dip on whichever surfaces are accessible is required to obtain a (relative) orientation, as described above. Where a structure was seen as a three-dimensional plane in a fragmented piece of core, or its trace could be observed at the top or bottom of a core section, the strike and a single apparent dip and dip direction were generally measured. When required, a thin (1-mm) sliver was shaved from oriented pieces of the working half of the core,

Table 8. Definitions of the fields in the working core description.

1. Core number and type.
2. Section number.
3. Piece number. A symbol of an x in a circle (⊗) is used if the piece is not oriented with respect to the vertical. Where a feature occurs on more than one piece it is recorded as the piece on which it was measured and the range of pieces on which it occurs is noted in the comments field.
- 4 and 5. Interval in centimeters that the feature covers on the cut face. Where the interval is less than 1 cm only the depth to top of the feature is recorded.
6. Feature. Type, e.g., vein, fracture, fault; and composition of material in structure (not on either side) e.g., fault gouge, vein fill. Abbreviations used are those defined in the metamorphic petrology section, this chapter.
7. Orientation of feature. Normally two apparent dips are measured and recorded in a dip direction/dip angle convention. The true dip is then calculated using a stereonet computer program and recorded in brackets on the sheet in dip angle/dip direction convention. If it is possible to measure the true dip directly, then that is recorded in the brackets without apparent dips. If the vertical axis on a non-oriented piece can be determined, apparent dips are recorded and true dip calculated as with the oriented pieces, but only the dip angle is recorded and a dash entered in place of the dip direction.
8. Shear/Method. Sense of movement and indicator, e.g., slickensides or rotated porphyroclasts, for faults and mylonitic zones.
9. Comments and sketches. Comments regarding the continuity and the form of the feature are usually recorded, as well as pertinent information on thickness, alteration halos, offsets, and crosscutting relationships. Fractures of the tiny white crack variety are noted by the initials TWC. If necessary, a sketch of the piece identifying the features is drawn. It is also noted by the initials HSD (hand specimen description) if a more detailed drawing and description of that piece has been done.

ODP Core Description:

STRUCTURAL GEOLOGY Leg. 140.....Site 504B...

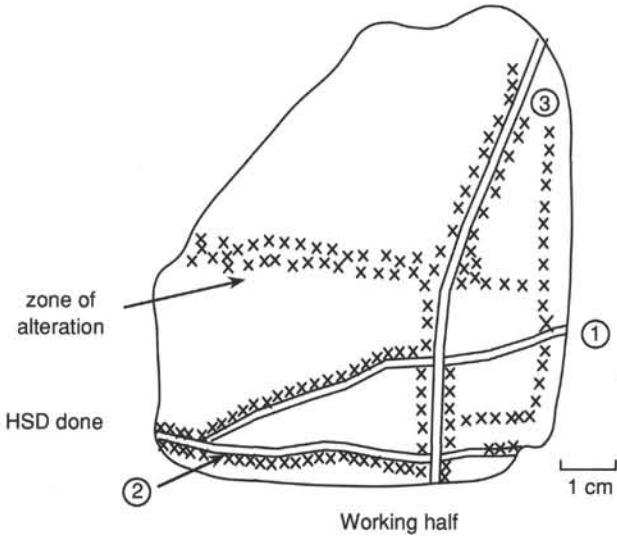
Core	Sec	Pieces	Interval		Feature		Orientation	Shear/method	Comments and Sketches
203R	1	15B	58	62	Vein	Chl	AD ₁ 270/71 AD ₂ 012/00 [71/282]		Planar surface of core
204R	1	3	12	13	Vein	Ac	AD ₁ 270/24 AD ₂ 000/06 [25/283]		<p>① Continuous, smooth, planar — sinuous intersects ③</p> <p>2 Planar, continuous, smooth intersects ③; relationship unclear — cut by ③ as shown by microscopic examination.</p> <p>③ Planar, continuous, smooth halo present cut by ① cuts ②</p> 
		3	13		Vein	Ac	AD ₁ 090/08 AD ₂ 000/04 [09/064]		
204R	1	3	7	14	Vein	Chl/Ac	AD ₁ 270/78 AD ₂ 354/00 [78/264]		

Figure 13. Example of working structural log used for recording discrete structural features.

ODP Core Description: DEFORMATION LOG

Leg..14Q... Site...504B

Core	Sec	Interval		Pieces	Deformation	Notes
185R	1	0	25	1–4	0	Lithology: OPC diabase
186R	1	0	150	1–18	0	Lithology: 1–6 (0–31 cm) OPC diabase 7 (31–35 cm) PC diabase 8–18 (35–150 cm) A diabase
186R	2	0	54	1–108	0	Lithology: A diabase
187R	1	0	64	1–14	0	Lithology: 1–13 (0–58 cm) P diabase 14 (58–64 cm) PC diabase
188R	1	0	41	1–12	0	Lithology: PC diabase
189R	1	0	146	1–28	0	Lithology: 1 (0–4 cm) PC diabase 2–28 (4–146 cm) OPC diabase
189R	2	0	117	1–16	0	Lithology: OPC diabase
190R	1	0	121	1–23	0	Lithology: OPC diabase
191R	1	0	150	1–25	0	Lithology: OPC diabase
192R	1	0	39	1–10	0	Lithology: OPC diabase
193R	1	0	65	1–14	0	Lithology: OPC diabase
194R	1	0	126	1–23	0	Lithology: OPC diabase
195R	1	0	10	1–3	0	Lithology: 1–2 (0–7 cm) OPC diabase 3 (7–10 cm) A diabase
196R	1	0	46	1–9	0	Lithology: 1 (0–6 cm) A diabase 2–9 (6–46 cm) OPC diabase
197R	2	0	143	1–19	0	Lithology: 1–22 (0–105 cm) OPC diabase 23–29 (105–143 cm) P diabase
197R	2	0	45	1–7	0	Lithology: P diabase
198R	1	0	85	1–21	0	Lithology: 1–17 (0–70 cm) P diabase 18–21 (70–185 cm) A diabase

Figure 14. Example of working deformation log used for recording variations in the style and intensity of ductile deformation.

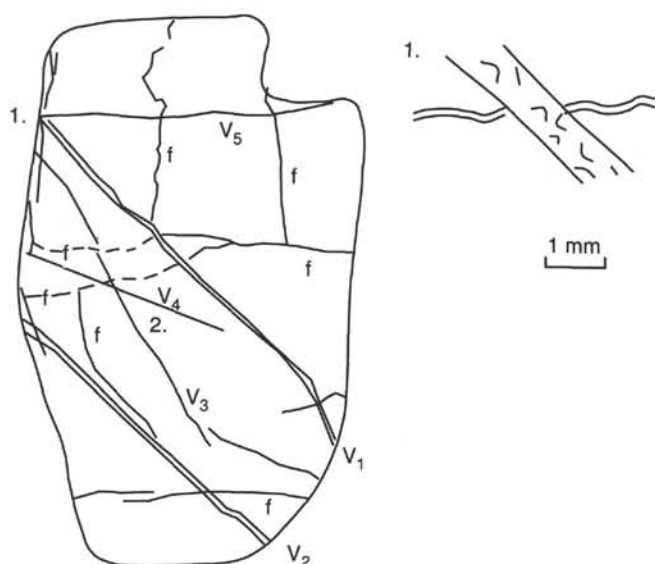
at the edge, orthogonal to the cut surface, providing a second surface from which apparent dips could be accurately determined. Dips recorded at this stage all assume that the core was vertical; if data from, e.g., the general purpose inclination tool (GPIT), suggest otherwise at a later stage, a correction can be made on the spreadsheet template. True dips were derived stereographically, using the Stereonet Plotting Program of R.W. Allmendinger, Version 4.1-11, (or Stereo program of D.B. McEachran, Version 5.12). The two apparent dip orientations were entered as lines, and the computer generated the great circle of cylindrical best fit to both lines. The orientation of this great circle gave the “working dip direction” and true dip of the

observed structure, which was recorded on the structural log, and also entered into the spreadsheet. In some small pieces the vertical axes could be identified from their cylindrical shape, but not the up direction, as they may have rolled in the core barrel (this was a particular problem for much of this leg, because no core liner was used). In these pieces the true dip of planar features was recorded, but not the direction of dip, which was meaningless.

Mineral foliations and lineations could be measured in much the same way as faults and veins, but as the cut surfaces are chosen to be parallel to lineations or perpendicular to foliations, they can often be measured as true orientations (none were encountered on this leg).

Core, section, piece	Oriented?	Top-bottom	Depth (mbsf)	Feature	Composition	Dir.	Angle	Dir.	Angle	Angle	Dir.	Mag. dec.	Mag. inc.	Angle	Dir.	Sense	SBA	Comments
173R-1, 2	Y	4-12	1570	Fracture		90	47	0	16	48	75						T	
173R-1, 6	Y	56-57	1570.6	Fracture		270	9											
173R-1, 12	Y	119-	1571.2	Fracture		90	2	180	15	15	173	129.6	-32.4	15	43.4		M	
173R-1, 12	Y	117-	1571.2	Fracture		90	4	180	14	15	164	129.6	-32.4	15	34.4		M	
173R-1, 13	Y	130-131	1571.3	Fracture		270	12	180	6	13	244							
173R-2, 3	Y	21-	1571.6	Fracture		270	2	180	7	7	196						T	
173R-2, 3	Y	19-27	1571.6	Fracture		90	77	0	80	82	37						T	
174R-1, 3	Y	17-19	1576.5	Fracture		270	76	155	0	77	245							
174R-1, 7	Y	47-48	1576.8	Fracture		270	81	170	0	81	260							
174R-1, 8	Y	50-57	1576.8	Fracture		90	75	278	0	78	128							
174R-1, 8	Y	50-55	1576.8	Fracture		270	63	123	0	74	213						T	
174R-1, 15	Y	95-96	1577.3	Fracture		270	30	180	25	37	231							
174R-1, 17	Y	109-110	1577.4	Fracture		270	20	180	25	31	218							
174R-1, 18	Y	117-118	1577.5	Fracture		90	4	0	0	4	90							
174R-2, 7	Y	34-36	1578.1	Fracture		270	38	180	6	38	262							
174R-2, 7	Y	37-38	1578.1	Fracture		270	29	180	0	29	270							
174R-2, 8	Y	42-44	1578.2	Fracture		90	14	180	1	14	94							
174R-2, 8	Y	42-46	1578.2	Fracture		270	32	0	25	38	307							
174R-2, 14A	Y	82-83	1578.6	Fracture		90	27	0	5	27	8							
174R-2, 14B	Y	85-	1578.6	Fracture		270	6	180	7	9	221						T	
175R-1, 3A	Y	11-12	1585.9	Fracture		90	20	180	8	21	111	29.7	-41.6	21	81.3		M	
175R-1, 3A	Y	14-15	1585.9	Fracture		90	6	180	4	10	143	29.7	-41.6	10	113.3		M	
175R-1, 3B	Y	19-22	1586	Dikelet?		270	57										T	1 mm lt minerals cut by fracture
175R-1, 3B	Y	20-21	1586	Fracture		270	3	0	14	14	348	29.7	-41.6	14	318.3		TM	
175R-1, 3A	Y	20-	1586	Vein	Chl					55	0	29.7	-41.6	55	330.3		M	
175R-1, 3A	Y	17-20	1586	Vein	Chl	90	65	180	41	67	112	29.7	-41.6	67	82.3		M	
175R-1, 5	Y	34-35	1586.1	Fracture		90	5	180	1	5	101							
175R-1, 5	Y	34-35	1586.1	Fracture		270	10											
175R-1, 5	Y	35-36	1586.2	Fracture		90	1	180	1	1	135							
176R-1, 18	Y	96-97	1596.3	Fracture		90	12	0	4	13	72							
176R-1, 18	Y	95-98	1596.3	Fracture		90	49	178	0	49	85							
176R-1, 20	Y	106-111	1596.4	Fracture		90	52											
176R-1, 20	Y	106-107	1596.4	Fracture		90	16	180	22	26	145							
176R-1, 24A	Y	128-129	1596.6	Fracture		90	21	180	1	21	93							
176R-1, 24B	Y	129-	1596.6	Fracture		270	11	180	6	13	152							
180M-, 5B, 1	Y	39-44	1618.8	Vein	Chl/Ac	90	70	115	0	81	25							<1 mm cont curvilinear
180M-, 5B, 1	Y	39-40	1618.8	Vein	Chl	270	9	197	0	9	287							<1 mm cont planar
180M-, 5A, 1	Y	39-40	1618.8	Vein	Chl	90	17	180	27	29	147							<1 mm cont planar
180M-, 6A, 1	Y	59-	1619	Vein	Chl/Ac	270	10	0	39	40	347							1 mm lt green core, cont, irreg, 3-5 mm alt halo
180M-, 7, 1	Y	72-76	1619.1	Fracture		270	48	0	28	51	295							
180M-, 7, 1	Y	76-79	1619.2	Fracture		0	15	270	38	40	289							
180M-, 7, 1	Y	73-77	1619.1	Vein	Chl	90	21	180	45	47	159							
180M-, 8, 1	Y	93-95	1619.3	Fracture		270	29	180	5	29	261	294.5	42.5	29	326.5		M	
180M-, 8, 1	Y	90-92	1619.3	Fracture		270	29	150	0	33	240	294.5	42.5	33	305.5		M	
180M-, 8, 1	Y	92-96	1619.3	Vein	Chl/Ac	90	30	180	60	61	162	294.5	42.5	61	227.5		M	
180M-, 1, 2	Y	0-10	1619.6	Vein	Ac/Chl	90	45	0	15	46	75							
180M-, 1, 2	Y	0-8	1619.6	Fracture		90	65	180	0	65	90							
180M-, 3, 2	Y	29-32	1619.9	Vein	Chl	270	3	0	32	32	355	329.1	-32.4	32	25.9		M	
180M-, 4, 2	Y	48-51	1620.1	Vein	Ac	270	4	180	35	35	186							
180M-, 4, 2	Y	48-50	1620.1	Vein	Ac	90	33	295	0	57	25							
180M-, 5, 2	Y	64-67	1620.2	Fracture		90	45	150	0	49	60							
180M-, 5, 2	Y	68-70	1620.3	Vein	Chl	90	50	180	18	51	105							
180M-, 7, 2	Y	96-97	1620.5	Fracture		270	47	180	7	47	264							
180M-, 7, 2	Y	96-97	1620.5	Fracture		90	45	180	10	45	100							
181M-, 7A, 2	Y	84-90	1622.7	Vein	Chl	90	73	160	0	74	70							
181M-, 12, 2	Y	147-148	1623.3	Vein	Chl	90	5	0	29	29	9	72.2	28.1	29	296.8		TM	
181M-, 12, 2	Y	146-147	1623.3	Vein	Ac/Chl	90	8	180	3	9	110	72.2	28.1	9	37.8		M	
181M-, 12, 2	Y	144-149	1623.3	Vein	Chl	270	80	180	42	80	261	72.2	28.1	80	188.8		TM	
186R-1, 5	Y	17-26	1626.5	Fracture		348	0	90	76	76	78						T	Continuous, planar, smooth. Actinolite?
186R-1, 5	Y	19-20	1626.5	Vein	Chl/Ac	270	5	180	27	27	190						T	Continuous, curvilinear, smooth.

Figure 15. Example of spreadsheet devised for the computer storage and manipulation of structural data derived from the core descriptions. See Appendix J in "Site 504" chapter (this volume).



140-504B-197R-2, Piece 2A

Comments:

Where fractures and veins intersect, fractures cut veins.

1. Chlorite-actinolite vein (V_1 , 1 mm), cuts a thinner (0.1 mm) chlorite-actinolite vein (V_5).

No offset is apparent, so either coincidental shear component parallel to early vein, or late vein thickens by assimilation of diabase and little dilation of fracture.

2. Chlorite vein (V_4 , 0.1 mm) cut by V_3 thicker chlorite-actinolite vein, slightly diffuse.

Figure 16. Example of hand specimen description form used for recording visual observation, such as crosscutting relationships.

Linear structures such as slickensides can be measured in a similar fashion: either directly, by their azimuth and amount of plunge, or indirectly, by means of their pitch on a previously measured plane. The sense of movement of linear structures can sometimes be ascertained, allowing distinction between components of normal vs. reverse and/or sinistral vs. dextral motion. The magnitude of displacement may be visible, and can be measured directly, if the fault surface is visible, or calculated from the apparent offset on the cut surface of the core.

Orientation of Core

Correction of the "working dip direction" to real geographical coordinates may be accomplished by use of both paleomagnetic and downhole logging data.

We have used the stable, high coercivity components of the magnetization measured from discrete minicores (see "Paleomagnetism" section, this chapter) as an external reference frame, but are well aware of the problems associated with such a procedure. The crust sampled at Hole 504B was formed at an oceanic spreading axis close to the equator. The upper crustal sequence carries a reversed magnetization, so the expected reference direction for the remanence is approximately horizontal and to the south. This may not necessarily be true for the lower crustal rocks, which may carry a normal remanence: this would introduce an error of 180° to the core orientation.

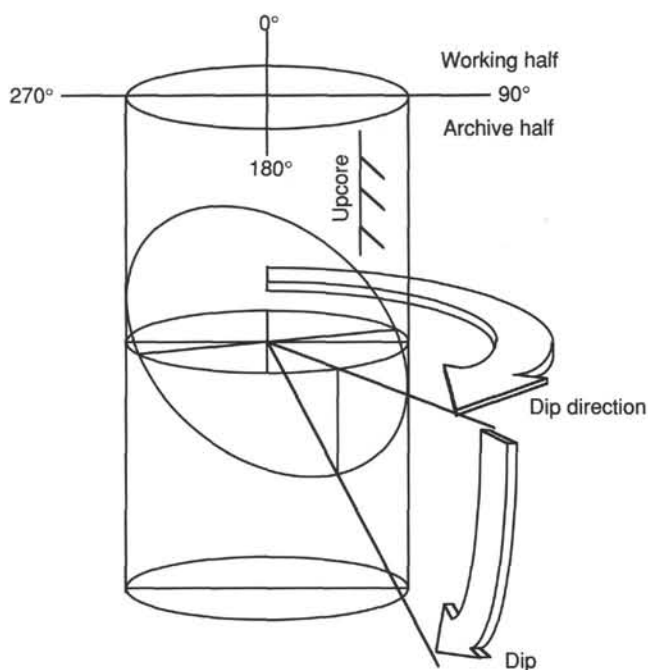


Figure 17. The convention used for the measurement of azimuths and dips on structural features in basement core.

Another problem involves the effect of a tilt on a paleomagnetic direction. In most situations a simple tilt about a horizontal axis will affect the declination as well as the inclination. We are fortunate that in the case of Hole 504B the major faults that are likely to cause tilting trend east, so that a south-trending magnetic vector would suffer only a minor shift in declination.

Within the plutonic sequence, rocks that carry a significant fabric can show deviation of the magnetic remanence away from the applied field due either to the influence of a previously existing magnetic fabric on the acquisition of the remanence or to a subsequent rotation effect. These processes are poorly understood, and difficult to correct. For this reason we suggest that, wherever possible, relatively isotropic rocks should be sampled.

The logging program on Leg 140 included the formation micro-scanner (FMS), a tool that makes an image of the borehole wall by measuring variations in resistivity by means of pads pressed against the wall (see "Downhole Measurements" section, this chapter). The FMS carries fluxgate magnetometers that allow orientation of the processed images. The FMS can be used in its own right as a structural tool, and is also of use in orienting sections of core. The difference between the diameter of the borehole and that of the core is such that identification of individual features on both cannot be made directly and may be difficult. The FMS tool can be used most successfully for orientation purposes when, for example, a single, regular joint or layering pattern can be recognized on downhole images and correlated with core-derived data.

Downhole logging is most powerful in this context when used in conjunction with paleomagnetism, as it potentially allows identification of possible tectonic rotations of the magnetization vector, which otherwise would have to be assumed to be zero.

Deformation Log

A continuous log of the style and intensity of the deformation was maintained. We have adapted the textural definitions used on Leg 118 (Dick et al., 1991) for the description of the plastic deformation structures in gabbros. We recognize 6 (0 through 5) classifications, in order of increasing grade of deformation:

0. Protolith: Original igneous grain relations observed, little or no grain shape anisotropy, plagioclase not obviously recrystallized.

1. Weakly foliated: Original igneous grain relations preserved, around 2:1 shape anisotropy, plagioclase partially recrystallized with clear coherent cores.

2. Strongly foliated: Some original igneous grain relations preserved around clinopyroxene, around a 4 to 5:1 clinopyroxene shape anisotropy, some recrystallized tails on pyroxene porphyroclasts, plagioclase mostly recrystallized.

3. Porphyroclastic mylonite: No original grain relations preserved in clinopyroxene, 8:1 clinopyroxene shape anisotropy with long recrystallization tails, all plagioclase recrystallized.

4. Mylonite: No original grain relations preserved, most clinopyroxene recrystallized, very fine grained, parallel banding often present.

5. Ultramylonite: Extreme grain-size reduction, few porphyroclasts present, not strongly foliated in hand specimen, dark color.

On this leg, pervasive deformation was slight, and only protolithic textures were encountered. These classes could, in most cases, be recognized in hand specimen, but were also checked in thin section. No direct relationship between percent deformation (% strain) and texture is implied. The relationship between the textural scale and percent deformation may be nonlinear and irregular, although it is clearly consistent with increasing degree of deformation and has the advantage that consistent observations can readily be made by different observers.

Thin-Section Descriptions

Thin-section billets of basement lithologies recovered during Leg 140 were examined (1) to confirm macroscopic descriptions of ductile and brittle structures; (2) to provide basic information on the kinematics of high-temperature ductile deformation and the effects of later brittle deformation; (3) to identify time relationships between deformation (ductile and brittle), magmatic, and alteration processes, and (4) to provide coverage of major structural zones and a representative section of downhole variations. Where possible, sections were oriented with respect to the core; i.e., the original attitude of the vertical is preserved, and in sheared or mylonitic zones samples were cut parallel to any extensional lineation and perpendicular to the

Leg: 140
Site: 504
Hole: B
Core: 198
Section: 1
Piece: 18
Interval: 70–71
Rock name:
Oriented: No

Observer: TAR, PTV.

Textural type: O.

Fabric: The high degree of alteration of the rock masks the original relationships between the igneous grains.

Recrystallization associated to ductile deformation: N/A.

Ductile: Plagioclase laths are slightly curved (primary feature). Amphibole crystals inside the veins are sometimes deformed (see sketch and comments).

Brittle: System of crosscutting veins with offset (see sketch and comments). En-echelon cracks in the chilled contact are related to shear deformation (see sketch and comments). Plagioclase laths are cracked.

Figure 18. Example of thin-section description form used for recording microscopic observations.

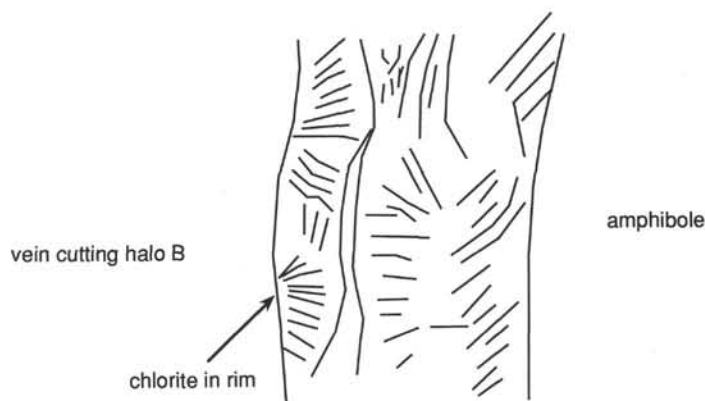
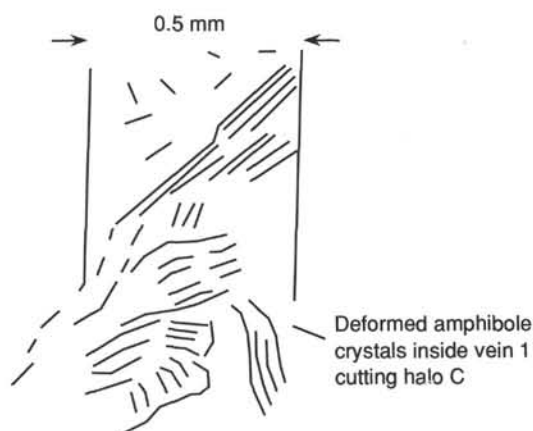
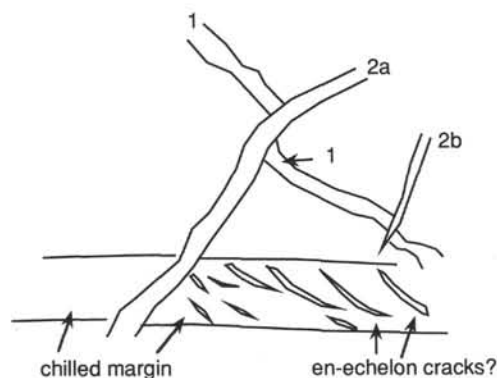
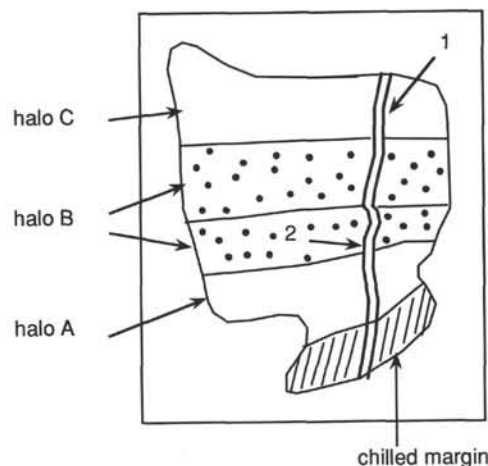
foliation for assessment of shear sense criteria. To ensure consistent and complete description of microscopic features a checklist was used for all thin sections described. This information was entered on a standardized format (Table 9). An example has been included in Figure 18. The results have been summarized in the site chapter (this volume, table 13), and important observations are included in the text. Copies of the original thin-section descriptions can be obtained from the ODP database if required.

Table 9. Definition of the elements of the standardized thin-section description.

Structural data to be recorded for thin-section descriptions
Leg:
Hole:
Core:
Section:
Piece:
Rock name:
Oriented?:
Observer:
Textural type: Type I, II, III, IV, V (according to Cannat et al., 1991). Textural type "0" has been introduced for rocks exhibiting no evidence for any planar or linear anisotropy, or incipient recrystallization.
Fabric: Primary characters γ (magmatic characters, if presents, e.g., cumulate; extent of preservation) γ ; γ defining minerals.
Plastic records, orientation; defining minerals.
Foliation; defining minerals.
Lineations; defining minerals.
Strength of preferred orientation (MacCaskie, 1986).
Recrystallization associated to ductile deformation: Degree of recrystallization for whole rock.
Degree for individual minerals; defining minerals.
Size of recrystallized grains, for each mineral.
Shape and grain boundaries.
Products of recrystallization.
Deformation structures:
Ductile: mechanical twinning, restricted mylonitic bands; shear bands; sigmoidal porphyroclasts/blasts; kinematic indicators.
Brittle: Fracturing of crystals and filling minerals, arrangement of the filling minerals; Fracturing of the whole rocks and filling minerals, arrangement of the filling minerals.
Veins on all scales and filling minerals, arrangement of the filling minerals.
Microfaults, sense of movement and offset.
Ductile/brittle: crosscutting relationships between veins, fractures, and mylonitic bands; time-relationships between ductile/brittle events.
Comments/sketches/photographs taken.

Comments/ sketches/ photos

140,504B, 198R-1, 70-71 cm, Piece 18.



Comments: Vein 2 accompanied by a broad (1.5 cm) halo which is lighter in color.

Vein 1, where cutting the rock outside the halo, consists mostly of dusty patches of amphibole. Where cutting the halo, the vein consists of clear patches of amphibole, with sparsely disseminated dusty patches. Vein 1 in general has complex composition. Thin clear discontinuous veins composed of colorless amphibole are included inside the vein. Along the edges of vein 1 there are irregular and discontinuous chlorite patches.

Fig. 18 (continued).

Conclusion

The various corrections to orientations and positions that were possible on board have led to the structural synthesis presented in the site chapter. Some of the interpretations will be refined after further work because, in addition to describing the cores, the structural geologists collected samples for shore-based analysis. An array of instrumental and analytical techniques will explore the nature of the

structures in detail. The emphasis while on board was on thorough and careful description of the range of structures observed.

PALEOMAGNETISM

Paleomagnetic measurements were performed on minicore samples and, in some cases, continuous pieces from the recovered core. Samples were chosen to be representative of the lithology and altera-

tion mineralogy of the Leg 140 cores and, when possible, were vertically oriented. At least one minicore sample was taken from each section of core for shipboard study. However, a few sections consisted only of small, unoriented fragments, and thus, were not sampled. For hard-rock cores, the only true orientation is with respect to the vertical dimension. This is because individual pieces of the core are free to rotate within the core barrel and thus are not oriented with respect to north, or to each other. However, subsequent to splitting individual pieces of the core, ODP convention for rotary cores follows that of an oriented piston core (see Fig. 19). That is, +X (north) is into the face of the working half of the core, +Y (east) points toward the right side of the face of the working half of the core, and +Z is down.

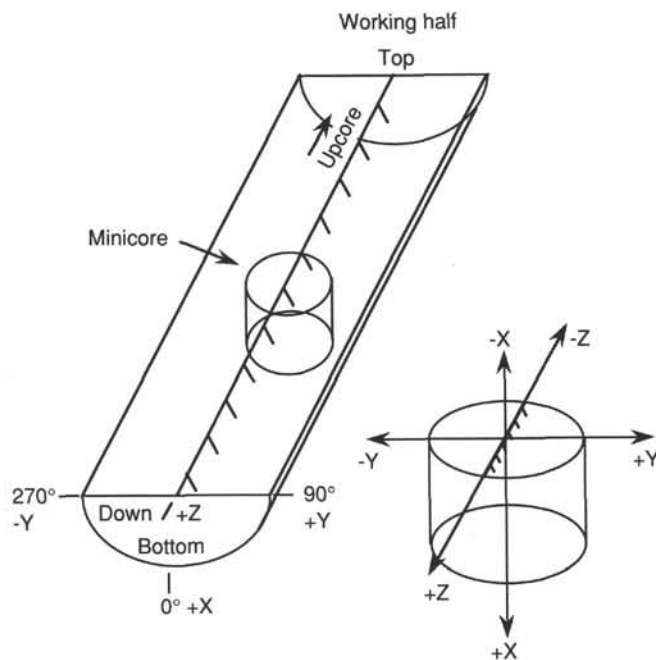


Figure 19. ODP paleomagnetic orientation convention.

Measurement of Remanent Magnetization

Two magnetometers, a Molspin spinner magnetometer and a 2-G Enterprises (Model 760R) pass-through cryogenic rock magnetometer, were used to measure remanent magnetization of the samples. The superconducting quantum interference device (SQUID) sensors in the cryogenic magnetometer measure the intensity and direction of magnetization over an interval approximately 20 cm long. During Leg 140, the SQUID electronics were operated in the flux-counting mode. An alternating field (AF) demagnetizer (Model 2G600), capable of producing an alternating field up to 20 mT, was used on-line with the pass-through cryogenic magnetometer. The magnetometer, the demagnetizer, and their common stepper motor transport system were operated over serial interfaces by software on an IBM PC compatible computer. The software was an ODP customization of a vendor (2-G) distributed QuicBasic program originally called SUPERMAG. Measurements of natural remanent magnetization (NRM) were taken after demagnetization levels of 2, 5, 7, 10, 15, and 20 mT.

AF demagnetization at higher fields was performed with a single-axis Schonstedt Geophysical Specimen Demagnetizer (Model GSD-1) at 25.0 and 30.0 mT and upward in 10-mT steps until the specimen decreased to below 10% of the NRM intensity and a stable inclination was identified.

Measurement of Magnetic Susceptibility

Magnetic susceptibility (K) of minicores was measured using a Bartington Magnetic Susceptibility Meter (Model MS1) using a 36-mm dual frequency loop in the low frequency mode. Values of initial susceptibility were used in conjunction with the values of the intensity of natural remanent magnetization (J_0) to calculate the Q ratio (Koenigsberger) of the samples. A field value of 0.033 mT was assumed for Site 504 so that $Q = J_0/(K \times 0.033)$.

Rock Magnetic Measurements

The relatively low recovery rate on Leg 140 gave us time to complete a series of rock magnetic measurements which are not standard procedure on ODP legs. We completed measurements of anhysteretic remanent magnetization (ARM), anisotropy of anhysteretic remanence (AAR), partial ARM (PARM), and isothermal remanent magnetization (IRM) on a representative set of minicores from the Leg 140 cores. Most of this additional work was done after the physical property measurements had been completed, during which the samples were heated to about 110°C, and this may have a limited effect on the magnetic properties of the samples (n.b., the bottom of the borehole is at about 195°C).

The ARM measurements were made using the Schonstedt AF demagnetizer and a DTECH, Inc., double-coil device, which allowed a steady, unidirectional field of 0.1 mT to be applied during each AF step. The ARM was acquired during progressive steps of increasing AF field, up to 90 mT, and the magnetization was measured in the cryogenic magnetometer between each step. The PARM measurements were made under the same experimental conditions, but the PARM was acquired in progressively increasing intervals, during the decay of a high demagnetizing field (e.g., ARM acquired in the 10–20 mT decay interval of a 500-mT AF field).

Anisotropy of anhysteretic remanence (AAR) gives a measure of the anisotropy of the ferromagnetic and ferrimagnetic minerals in the rock (in contrast to anisotropy of magnetic susceptibility, which is also influenced by the diamagnetic and paramagnetic minerals). Selected samples, chosen for their equant dimensions (i.e., as broad as they are long), were first demagnetized in three orthogonal axes at 90 mT. An ARM was then acquired along the +X axis in a direct field of 0.1 mT and an alternating field of 50 mT. Each sample was measured on the cryogenic magnetometer, and then demagnetized in three axes at 60 mT. This procedure was repeated for five other positions: (1) +Y, (2) +Z, (3) +X and +Y, (4) +X and +Y, and (5) +Y and +Z. This gave sufficient redundancy in the determination of the six unknowns in the anisotropy ellipsoid:

$$\begin{aligned} K &= [K_{xx}, K_{xy}, K_{xz}] \\ K &= [K_{xy}, K_{yy}, K_{yz}] \\ K &= [K_{xz}, K_{yz}, K_{zz}] \end{aligned}$$

to be accomplished by a standard least squares technique. The eigenvalues and eigenvectors of the matrix, K , were determined to give the magnitude and orientations of the principal axes of the ellipsoid. A standard error was calculated from the residuals of the least squares fit, which gave an estimate of the quality of the data. The error was also expressed as a percentage of the magnitude of the intermediate anisotropy axis.

The IRM acquisition experiments were accomplished using the ASC Scientific Impulse Magnetometer (Model IM-10). Samples were subjected to a steady magnetic field along the +X axis and measured with the Molspin spinner magnetometer. This process was repeated for progressively increasing fields, up to 1.2 T. The backfield IRM was then determined by applying a progressively increasing

steady field in the $-X$ axis, until the sample intensity in the X axis was reduced to below 0 mA/m.

PHYSICAL PROPERTIES

Compressional-wave velocities, index properties (bulk density, porosity, water content, and grain density), and thermal conductivities were measured on the crystalline rocks recovered during Leg 140. Experimental details are described below and in the cited references.

Compressional-wave Velocity

The pulse transmission method was employed to determine the compressional-wave velocity using piezoelectric transducers as sources and detectors in a screw-press Hamilton Frame described by Boyce (1976). Calibration measurements were performed using plexiglas and aluminum minicores to determine the zero displacement time delay inherent in the measuring system. The traveltimes through a range of different lengths of each material were measured (Table 10) and plotted on a time-distance graph. An average of the intercept at zero length for both materials gives the delay time for the particular set of transducers (Fig. 20). This technique has been previously used for measurements in Hole 504B (Shipboard Scientific Party, 1988a) and is preferable to taking a single reading at zero length. Early tests indicated that the flatness and parallelism of the specimens determined the accuracy and reproducibility of the measurements. Accordingly, the samples were prepared with both sides flat and parallel to within 0.08 mm. This small tolerance resulted in sharply defined first arrivals of the direct P -wave mode.

Table 10. Calibration measurements for the thermal conductivity needle probes.

	Thickness (mm)	Traveltime (μ s)
Plexiglas	10.00	5.865
	20.05	9.725
	37.93	16.610
	50.09	21.140
	65.72	26.970
	for $x = 0$ mm, $t = 2.122$ μ s	
Aluminum	20.50	5.555
	30.00	7.260
	39.98	8.830
	50.16	10.775
	60.44	12.340
	for $x = 0$ mm, $t = 2.160$ μ s	
Average delay time = 2.141 μ s		

Shipboard compressional-wave velocity measurements are usually obtained in three orthogonal directions (A, B, and C transmission directions) as shown in Figure 21. Due to sampling limitations, only two types of minicores (25.3 mm in diameter and 15–40 mm long) were used during Leg 140: (1) samples drilled vertical or parallel to the core axis (pulse transmission A) and; (2) normal to the core splitting plane (i.e., horizontal) and usually at an angle to foliation (pulse transmission C). Measurement uncertainties in transmission length (± 0.08 mm, $\pm 0.25\%$ of length) and timing uncertainties (± 0.035 s or 0.1%) yielded nominal uncertainties in V_p of about 0.3%. Calibration against standards (leucite $V_p = 2.745$ km/s and silica glass $V_p = 5.97$ km/s) were reproduced to within 0.3%. Measurement of V_p in an aluminum standard resulted in a velocity of 6.125 ± 0.035 km/s, about 2% lower than the nominal velocity of 6.295 km/s. In practice, heterogeneity of the rock samples and irregularities in the sample shapes and finishes degrade the experimental accuracy to about 0.8% or 5×10^{-2} km/s.

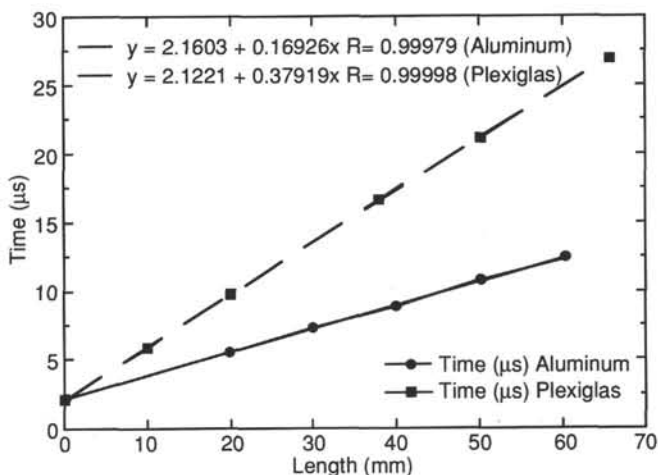


Figure 20. Calibration plot used for the Hamilton Frame velocimeter.

Index Properties

Wet and dry densities, porosities, and water contents were determined on all the minicore samples using a motion-compensated microbalance measurement of mass (± 0.002 g accuracy) and a Penta-pycnometer measurement of sample volumes ($\pm 0.03\%$) in both the saturated and dry states. The Penta-pycnometer is specifically designed to measure the volume and true density of the samples by employing Archimedes' principle of fluid displacement. The displaced fluid is helium, which assures penetration into crevices and pores approaching one Angstrom (10^{-10} m) in dimension. Problems with wet samples have been previously reported (Scientific Shipboard Party, 1988a) because helium tends to dissolve in the pore water giving rise to low volume determinations. Purge times of 5 min were used to approach a helium-saturated steady state condition. After measuring the wet volumes and calculating the bulk densities, samples were dried at $110 \pm 5^\circ\text{C}$ for 24 hr. Purge times of 5 min were

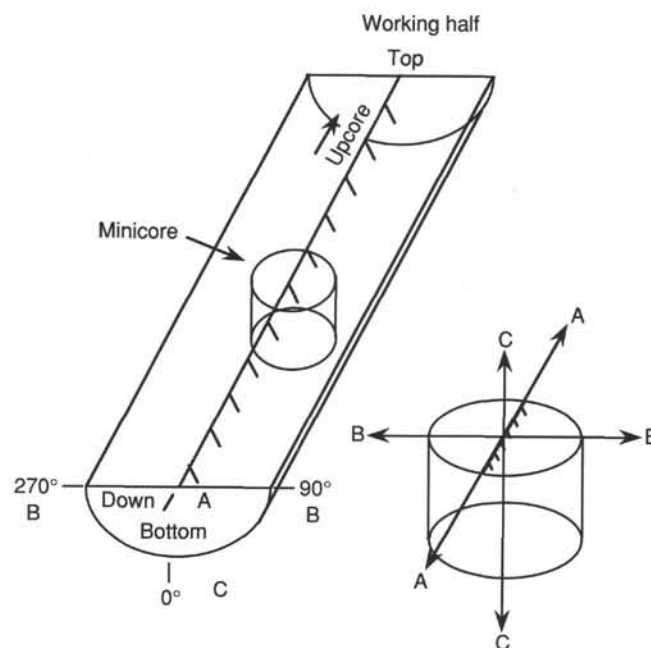


Figure 21. Orientation diagram and terminology used for physical properties measurements.

also used, and overall accuracies of bulk and grain densities are about 0.2% or $6 \times 10^{-3} \text{ g/cm}^3$. Porosities were determined to probably no better than $\pm 0.2\%$, assuming that the porosity is interconnected and fluid saturated.

Thermal Conductivity

Core samples were measured nondestructively for thermal conductivity in the shipboard laboratory. Specimens were obtained from the archive half in order to keep samples used for chemistry analyses from being contaminated with thermal conductive grease. This technique was previously used during Leg 129 and is documented in the shipboard thermal conductivity manual. Measurements were performed over 5 min with a heated needle probe sandwiched between the sample and a slab of low-conductivity material (Vacquier, 1985). This method is most convenient for the hard-rock cores, which were cut in the form of a half-round cylinder because this shape is easily adapted to the apparatus. The flat end was then polished, in order to provide a good thermal coupling surface between the sample and the needle probe.

The theory of the method closely approximates the heating of a line source in a plane separating half-spaces of the sample material and a thermal insulator, which in turn is a relatively straightforward extension of the method of heating a uniform full-space by a line source (Jaeger, 1956; Von Herzen and Maxwell, 1959). If the substrate on which the sample is placed were a perfect thermal insulator, the rise in temperature with time at the needle probe would be exactly twice that experienced by the probe in an infinite medium having the same thermal conductivity of the sample. The thermal conductivity is then estimated by calculating the slope of the best-fit straight line to a plot of temperature vs. the natural logarithm of time, where the value of the slope is inversely proportional to the conductivity. Specifically, the data are fit to the following equation:

$$T = (q/4 \times \pi \times k) \ln(t) + At + B,$$

where T is the temperature, q is the heat input to the sample per unit length per unit time, and k is the conductivity. In practice, the poorly conducting substrate absorbs a fraction of the heat during measurement, the amount of which depends on the ratio of sample to substrate conductivity. For most rock samples measured during Leg 140, this ratio was sufficiently large (>15 – 20) that the adjustment from the simple theory require a relatively small correction. This correction was determined by carefully measuring materials whose conductivity was known and close to those measured in the samples.

Measurements of rock thermal conductivity by this technique were conducted sporadically during previous ODP legs. Measurements on 9 basalt samples were reported from Leg 109, Hole 648B (Shipboard Scientific Party, 1988b), as well as from Leg 111, Hole 504B (Shipboard Scientific Party, 1988a), and 38 gabbro samples from Leg 118, Hole 735B (Shipboard Scientific Party, 1989). These studies indicated that the multiplying factors used to convert the conductivity value calculated from the full-space theory to the actual value represented by the samples ranged from 2.1 to 2.7, apparently depending on the time period used after initiation of the transient experiment. These factors were obtained by comparing well-established conductivity values for standard materials determined over the same time periods in the same apparatus (Table 11).

Before measuring the samples obtained from this hole, 60 measurements were performed using red and black rubber half-rounds and a slab of synthetic material designated as "macor" on each needle-probe. These measurements were run over a transient needle-probe heating duration of 6 min to determine the best period during which data should be obtained. Almost all the standard measurements produced the same heating pattern with an initially steep slope of temperature vs. \ln time over the first 60–90 s, gradually decreasing to a

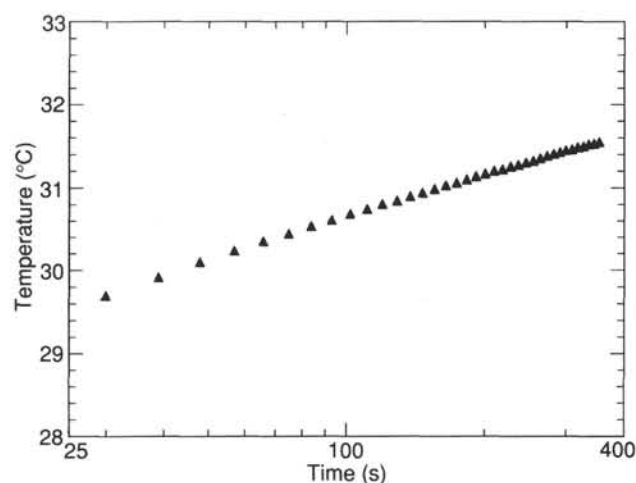


Figure 22. Typical plot of a thermal conductivity measurement using the needle probe and the half-space method. Note the more uniform slope after 60 s.

more uniform slope (Fig. 22). Most measurements of core samples from this hole showed the same characteristics. To reduce the effects of any external temperature changes, all calibration runs were conducted when the temperature of the standard bath was changing at a rate less than 0.01°C/min .

After measuring the thermal conductivity of the standards, it was determined that the red rubber and the macor gave the most reliable results. Also, the conductivity values calculated with two of the needle probes (#207 and #205) produced values within the standard error of the measurements (Table 11). These analyses suggested that the multiplying factors, used to convert the conductivity values calculated from the full-space theory, were best obtained during a time period between 60 and 240 s.

DOWNHOLE MEASUREMENTS

Measurement Descriptions

Downhole measurements determine the physical, chemical, and structural properties of formations adjacent to the borehole. Interpretation of these continuous, in-situ measurements can yield a stratigraphic, lithologic, structural, geophysical, and geochemical characterization of the hole. After coring is completed, a combination of sensors are lowered downhole on a seven-conductor cable, and each of several measuring devices continuously monitors the properties of the formations present. Of the dozens of different combinations commonly used in the petroleum industry, six combinations of downhole sensors were used on Leg 140: (1) a high-resolution temperature tool, (2) the geophysical combination, (3) the geochemical combination, (4) the formation microscanner (FMS), (5) the borehole televiewer (BHTV), and (6) a flowmeter.

Leg 140 represented an outstanding opportunity to determine the temperature profile in the upper part of Hole 504B, where a renewed vigorous downflow of seawater was detected during Leg 137, only 6 months prior to this experiment. The downhole sensor was essentially the same as that used about 5 years earlier by Gable et al. (1989) to record temperature data during Leg 111.

The geophysical combination used on Leg 140 consisted of the dual laterolog tool (DLL), the sonic tool (LSS), and the lithodensity tool (LDT). This tool combination measures electrical resistivity, compressional-wave velocity, formation density, and photoelectric effect. The geochemical combination consists of a natural gamma-ray spectrometry tool (NGT), an aluminum clay tool (ACT), and an induced gamma-ray spectrometry tool (GST). This tool combination

measures the relative concentrations of 11 elements, including aluminum, silicon, calcium, iron, sulfur, manganese, hydrogen, chlorine, potassium, thorium, and uranium.

The FMS is a microelectrical imaging device designed and operated by Schlumberger. It allows for visual characterization of the structures met in the near vicinity of the borehole wall from measurements related to the formation's electrical conductivity. The geophysical combination, the geochemical combinations, and the FMS microelectrical imaging device are supplied and operated on board the *JOIDES Resolution* by Schlumberger.

The BHTV is an ultrasonic imaging device which produces a map of acoustic properties of the borehole surface. The downhole flowmeter was deployed successfully for the first time in Hole 504B. Previous attempts had not succeeded due to failures (1) to keep the downhole packer inflated in casing (Leg 137), and (2) to transmit downhole the pressure generated by the rig pumps (Leg 139). Both for safety reasons and in order to maximize the chances of success of the experiment, the strong downflow of ocean bottom water into Hole 504B observed during Leg 137 (and earlier DSDP/ODP legs at this site) was used to perform the flowmeter measurement.

Measurement Devices

A brief description of in-situ sensors used during Leg 140 is given below. A more detailed description of the physical principles of these sensors and their applications is provided by Hearst and Nelson (1984) and Ellis (1987).

Temperature

During Leg 140, the high-resolution temperature tool designed at the Bureau de Recherche Géologiques et Minières (BRGM), France, was used immediately after the first re-entry into Hole 504B. The measurements were recorded in the upper 500 m of the hole (about 85°C), as particular attention was paid to the renewed, and unexpected, flow of ocean-bottom water in the upper part of the basement observed during Leg 137. The temperature sensors are accurately calibrated thermistors housed in a 5-mm-diameter tube at the lower end of the probe. Temperatures are determined from the resistance of two thermistors that can be monitored separately or in combination for maximum sensitivity.

Electrical Resistivity

The dual laterolog instrument (DLL) provides three different measurements of electrical resistivity, each with a different radial depth of investigation. The DLL measures the intensity of a variable current focused in a 60-cm-thick cylindrical beam, while flowing from a downhole electrode to a remote return under a fixed difference of potential. The intensity of the measured current is inversely proportional to the formation resistivity. This sensor remains accurate at high resistivity values (with an error <1.0% up to 40,000 ohm-m). It provides two measurements of resistivity referred to as "deep" and "shallow" on the basis of the respective depths of horizontal penetration of the current into the rock from the axis of the borehole. An estimate of the fracture porosity and orientation can be computed in crystalline rock from these two measurements. The vertical resolution of the DLL is of the order of 0.60 m.

To a first-order approximation, resistivity responds to the inverse square root of porosity (Archie, 1942). In addition, water salinity, clay content, and temperature are important factors controlling the electrical resistivity of rocks. Other factors that may influence the resistivity of a rock include the concentration of clays, magnetite, ilmenite, and sulfide minerals, the presence of vesicles, and the geometry of interconnected pore spaces.

Sonic Velocity

The digital sonic measurement (LSS) uses two acoustic transmitters and two receivers to measure the time required for sound waves to travel along the borehole wall over source-receiver distances of 2.4, 3.0, and 3.6 m. The raw data are expressed as the time required for a sound wave to travel through 0.31 m of formation; these traveltimes are then converted to sonic velocities. First arrivals for the individual source-receiver paths are used to calculate the velocities of the different waves traveling in the formation (compressional, shear, surface, etc.). Only compressional-wave velocity is determined on board the ship; the full sonic waveforms are recorded for post-cruise processing to determine shear wave and Stoneley wave velocities. The vertical resolution of the tool is 0.61 m. Compressional-wave velocity is primarily controlled by porosity and diagenesis; increases of these two factors generally cause velocity to increase.

Lithodensity Measurement

The lithodensity tool (LDT) uses a ^{137}Cs gamma-ray source to measure the back-scattered flux at fixed distances from the source. Under normal operating conditions, attenuation of gamma rays is chiefly caused by Compton scattering (Ellis, 1987). Formation density is extrapolated from this energy flux by assuming that the atomic weight of most rock-forming elements is approximately twice the atomic number. A photoelectric effect factor (PEF) is also provided. Photoelectric absorption occurs in the energy window below 150 keV and depends on the energy of the incident gamma ray, the atomic cross section, and the nature of the atom. This measurement is almost independent of porosity and can therefore be used directly as a matrix lithology indicator. The radioactive source and detector array are placed in a tool that is pressed against the borehole wall by a spring-loaded caliper arm. Excessive roughness of the borehole wall allows drilling fluid between the skid and the formation and, consequently, the density measurement will give rise to false low values in such a setting. Approximate corrections can be applied using caliper data. The vertical resolution of the measurement is about 0.30 m.

Gamma-ray Spectrometry Measurement

This induced gamma-ray device (GST) consists of a pulsed source of 14-MeV neutrons and a gamma-ray scintillation detector. The GST uses prompt neutron capture, in which an atom captures a thermal neutron, becomes unstable and decays instantaneously, emitting gamma rays of capture which are recorded to provide a raw gamma-ray spectrum. A surface computer performs spectral analysis on the latter. Characteristic sets of gamma rays from six elements dominate the spectrum: Ca, Si, Fe, Cl, H, and S. As their sum is always unity, they do not reflect the actual elemental composition. Consequently, ratios of these elements are used in interpreting the lithology and porosity of the formation and the salinity of the formation fluid.

Aluminum-Clay Measurement

Aluminum abundance as measured by the aluminum clay tool (ACT) is determined by neutron-induced (^{252}Cf source) gamma-ray spectrometry. The contribution to the gamma-ray spectrum by natural radiation is removed by placing NaI gamma-ray detectors above and below the neutron source; the one above measures the natural radiation before activation, and the one below the induced radiation after activation. It is then possible to subtract the naturally occurring component from the total measured after activation. Calibration to elemental weight percent (wt%) is performed by taking irradiated core samples of known volume, density, and composition, and measuring their gamma-ray output while placed in a jig attached to the tool.

Table 11. Calibration measurements for the thermal conductivity needle probes.

Needle #205 pos 1 red rubber
 Needle #206 pos 2 black rubber
 Needle #207 pos 3 macor

Run #	Window	Pos 1	Std Error	Window	Pos 2	Std Error	Window	Pos 3	Std Error
455	63–243	0.992	0.006	66–246	0.596	0.005	69–249	1.626	0.007
456	63–243	1.005	0.007	66–246	0.538	0.008	69–249	1.648	0.006
457	63–243	1.018	0.006	66–246	0.507	0.03	69–249	1.622	0.006
458	63–243	0.994	0.006	66–246	0.566	0.022	69–249	1.626	0.008
459	63–243	0.954	0.011	66–246	0.58	0.027	69–249	1.616	0.007
460	63–243	0.992	0.006	66–246	0.731	0.018	69–249	1.687	0.006
461	63–243	0.979	0.008	66–246	0.556	0.007	69–249	1.622	0.006
462	63–243	0.988	0.008	66–246	0.594	0.009	69–249	1.586	0.006
463	63–243	0.986	0.008	66–246	0.628	0.007	69–249	1.578	0.005
464	63–243	0.985	0.006	66–246	0.636	0.009	69–249	1.623	0.007
465	63–243	1.02	0.008	66–246	0.57	0.034	69–249	1.697	0.010
466	63–243	1.034	0.008	66–246	0.687	0.011	69–249	1.776	0.008
467	63–243	0.99	0.007	66–246	0.601	0.009	69–249	1.654	0.007
468	63–243	0.996	0.005	66–246	0.69	0.02	69–249	1.651	0.006
469	63–243	1.035	0.009	66–246	0.751	0.03	69–249	1.658	0.007
470	63–243	0.987	0.011	66–246	0.689	0.03	69–249	1.612	0.007
471	63–243	1.006	0.007	66–246	0.559	0.031	69–249	1.617	0.007
472	63–243	1.017	0.005	66–246	0.547	0.029	69–249	1.609	0.003
473	63–243	1.031	0.007	66–246	0.654	0.004	69–249	1.659	0.007
474	63–243	1.012	0.005	66–246	0.621	0.005	69–249	1.678	0.006
	Mean	1.001	0.007		0.615	0.017		1.642	0.007
	Std	0.021	0.002		0.067	0.011		0.044	0.001

Needle #205 pos 1 macor
 Needle #206 pos 2 red rubber
 Needle #207 pos 3 black rubber

Run #	Window	Pos 1	Std Error	Window	Pos 2	Std Error	Window	Pos 3	Std Error
476	63–243	1.667	0.006	66–246	1.007	0.007	69–249	0.652	0.009
477	63–243	1.628	0.005	66–246	0.742	0.018	69–249	0.662	0.005
478	63–243	1.606	0.006	66–246	0.713	0.016	69–249	0.655	0.463
479	63–243	1.658	0.005	66–246	0.762	0.02	69–249	0.658	0.005
480	63–243	1.569	0.004	66–246	0.824	0.012	69–249	0.657	0.006
481	63–243	1.514	0.006	66–246	0.851	0.018	69–249	0.671	0.008
482	63–243	1.595	0.005	66–246	0.995	0.013	69–249	0.663	0.009
483	63–243	1.605	0.007	66–246	1.162	0.013	69–249	0.661	0.009
484	63–243	1.619	0.005	66–246	0.904	0.017	69–249	0.668	0.008
485	63–243	1.556	0.006	66–246	1.014	0.016	69–249	0.674	0.005
486	63–243	1.56	0.006	66–246	0.941	0.005	69–249	0.66	0.007
487	63–243	1.575	0.006	66–246	0.895	0.006	69–249	0.659	0.007
488	63–243	1.563	0.008	66–246	0.906	0.006	69–249	0.67	0.007
489	63–243	1.628	0.005	66–246	0.973	0.026	69–249	0.668	0.005
490	63–243	1.598	0.005	66–246	0.897	0.023	69–249	0.668	0.005
491	63–243	1.619	0.005	66–246	1.146	0.021	69–249	0.665	0.009
492	63–243	1.576	0.005	66–246	0.872	0.008	69–249	0.661	0.009
493	63–243	1.623	0.006	66–246	1.116	0.021	69–249	0.659	0.006
494	63–243	1.596	0.006	66–246	1.027	0.023	69–249	0.667	0.006
495	63–243	1.59	0.005	66–246	1.088	0.017	69–249	0.677	0.007
496	63–243	1.667	0.005	66–246	0.914	0.009	69–249	0.667	0.005
	Mean	1.597	0.006		0.937	0.016		0.665	0.03
	Std	0.036	0.001		0.129	0.006		0.006	0.102

Natural Gamma-ray Measurement

The natural gamma-ray tool (NGT) measures the natural radioactivity of the formation. Most gamma rays are emitted by the radioactive isotope ^{40}K and radioactive isotopes of the U and Th decay series. The gamma radiation originating in the formation close to the borehole wall is measured by a scintillation detector mounted inside the sonde. The analysis is achieved by subdividing the entire incident gamma-ray spectrum into five discrete energy windows. The total counts recorded in each window, for a specified depth in the well, are processed at the surface to give elemental abundances of K, U, and Th.

Borehole Inclination and Magnetometer Measurement

The general purpose inclination tool (GPIT) contains a three-component accelerometer and a three-component magnetometer. The

device is used to measure the orientation of the downhole sensors within the borehole, and the orientation (or deviation) of the borehole itself, as well as to compensate for instrument accelerations in the axis of the borehole during data acquisition. It is included as a part of the FMS. From the three-axis magnetometer data, a derivation of the magnetic inclination, declination, and total field can be obtained.

FMS Electrical Images

The formation microscanner (FMS) produces high-resolution borehole images from electrical conductivity measurements (Ekstrom et al., 1986). Designed for oil exploration purposes in the early 1980's, the use of the FMS was initially precluded in the Ocean Drilling Program because of diameter constraints imposed by the internal diameter of the drill pipe (4.125 in.). A modified, smaller diameter FMS was consequently developed by Schlumberger for ODP. The

Table 11 (continued).

Needle #205 pos 1 black rubber									
Needle #206 pos 2 macor reported									
Needle #207 pos 3 red rubber									
Run #	Window	Pos 1	Std Error	Window	Pos 2	Std Error	Window	Pos 3	Std Error
497	63-243	0.788	0.006	66-246	1.58	0.006	69-249	0.952	0.008
498	63-243	0.77	0.005	66-246	1.763	0.012	69-249	0.967	0.005
499	63-243	0.788	0.012	66-246	1.465	0.019	69-249	0.956	0.005
500	63-243	0.786	0.007	66-246	1.618	0.028	69-249	0.966	0.005
501	63-243	0.762	0.009	66-246	1.536	0.006	69-249	0.941	0.007
502	63-243	0.767	0.004	66-246	1.729	0.018	69-249	0.941	0.004
503	63-243	0.786	0.007	66-246	1.536	0.005	69-249	0.952	0.004
504	63-243	0.776	0.007	66-246	1.447	0.004	69-249	0.959	0.006
505	63-243	0.773	0.017	66-246	1.188	0.024	69-249	0.896	0.006
506	63-243	0.791	0.013	66-246	1.337	0.023	69-249	0.985	0.007
507	63-243	0.739	0.009	66-246	1.551	0.027	69-249	0.943	0.006
508	63-243	0.813	0.012	66-246	2.138	0.029	69-249	0.959	0.005
509	63-243	0.813	0.009	66-246	1.436	0.019	69-249	0.967	0.005
510	63-243	0.778	0.019	66-246	2.138	0.021	69-249	0.959	0.005
511	63-243	0.765	0.008	66-246	2.305	0.023	69-249	0.967	0.006
512	63-243	0.787	0.014	66-246	1.788	0.011	69-249	0.965	0.008
513	63-243	0.757	0.011	66-246	1.996	0.02	69-249	0.949	0.007
514	63-243	0.781	0.006	66-246	1.978	0.028	69-249	0.975	0.005
515	63-243	0.791	0.011	66-246	1.905	0.007	69-249	0.988	0.007
516	63-243	0.797	0.011	66-246	1.734	0.01	69-249	0.976	0.007
	Mean	0.781	0.010		1.708	0.017		0.958	0.006
	Std	0.018	0.004		0.295	0.009		0.02	0.001

Note: The following standards were used on all three needle probes: (1) red rubber with a reported thermal conductivity (TC) of $0.96 \pm 0.05 \text{ W/m}\cdot\text{K}$; (2) black rubber with a reported TC of $0.54 \pm 0.02 \text{ W/m}\cdot\text{K}$; and (3) macor with a TC of $1.61 \pm 0.08 \text{ W/m}\cdot\text{K}$. All values for the standard materials were provided by the U.S. Geological Survey. Pos = position; Std = standard.

FMS has a vertical resolution of approximately 1.0 cm, but a detection threshold for conductive features on the order of micrometers. With this fine-scale detection ability (raw data points are recorded every 2.5 mm), it allows detailed study of subsurface structures. This compares with typical conventional downhole measurements that are averaged over 150 mm; the sampling rate of the FMS is consequently 60 times larger than most other logging devices. The FMS has four orthogonal pads that are pressed against the borehole wall with spring-loaded arms.

The new FMS was designed in such a way that each of the four pads carries an array of 16 closely spaced electrodes. The electrode currents probe the conductivity of the rock to a depth of a few centimeters into the borehole wall, thus responding to such variations in physical and chemical properties of the rock as porosity or surface conduction when conductive clay minerals such as smectites are present. The series of conductivity traces are displayed side by side, then coded into an image where black represents the most conductive values and white the most resistive ones. The four images (of 16 traces each) are recorded simultaneously. Once the data have been acquired in the borehole, the images are processed on a dedicated workstation to allow for on-site comparison with the cores. Possible applications of the FMS-derived images include detailed correlation of coring and logging depth, orientation of cores, identification and mapping of fractures, faults, foliations, as well as determining strike and dip of structures (Pezard and Luthi, 1988; Pezard et al., 1988).

The FMS can also be used to determine in-situ principal horizontal stress directions from the precise measurement of two orthogonal calipers. In an isotropic, linearly elastic rock subject to differential stresses, breakouts form along the borehole wall as a result of compressive stress concentrations exceeding the strength of the rock. Under these conditions, the breakout orientation develops in the direction of least principal horizontal stress. It has been demonstrated in different areas that stress orientations deduced from breakouts are consistent with other independent indicators (Bell and Gough, 1979; Morin et al., 1990).

BHTV Acoustic Images

The digital borehole televiewer (BHTV) is an ultrasonic tool designed by Deutsche Montan Technologie (DMP), Germany, that produces an acoustic image of the borehole wall. A transducer emits ultrasonic pulses which are reflected at the borehole wall. The same transducer also records the reflected signal. The BHTV then electronically analyzes the incoming signal. Amplitude and traveltime of the reflected signals are stored in the logging computer. While the transducer rotates and the tool moves upward, information on the entire borehole wall and borehole shape are recorded, leading finally to an unwrapped image of the borehole wall both in amplitude and time. The digital BHTV used on this leg for open hole measurements differs from the analog BHTV which was used in previous downhole measurements in Hole 504B.

The amplitude of the reflected signal depends on the reflection coefficient of the borehole fluid-rock interface, the position of the BHTV tool in the borehole, the shape of the borehole, and the roughness of the borehole wall. Especially, changes in the borehole wall roughness are responsible for the modulation of the reflected signal. Fractures or changes in the drilled rocks can easily be recognized in the amplitude image. On the other hand, the recorded traveltime images give detailed information about the shape of the borehole, as 128 signals are recorded per revolution. The BHTV can thus be considered as a very sophisticated "caliper log," and used to determine the principal horizontal stress directions. As amplitude and traveltime are recorded together with a pointer to magnetic north, it is possible to display the oriented data and to get a complete image of the borehole wall. Like the FMS, this downhole sensor can thus be used to re-orient cores.

Flowmeter Experiment

Permeability is the key physical property controlling fluid transport and exchange processes in the ocean crust. To date, the drill-string packer system (Becker et al., 1989) is the only method which was successfully used onboard ship by DSDP/ODP to measure the in-situ

permeability of the ocean crust. The first application of this standard hydrologic field technique to the marine environment occurred at Hole 504B during DSDP Leg 69 (Anderson and Zoback, 1982). Since that initial effort, the method has emerged as a reliable and indispensable part of several other downhole measurements programs which have shared a common hydrogeologic research theme (Hickman et al., 1984; Becker et al., 1983). In the case of Hole 504B, a systematic program of packer testing has been performed during Legs 69, 83, 92, and 111. These data provide a representation of the vertical distribution of bulk permeability in the oceanic crust at this site to 1500 mbsf (Anderson et al., 1985; Becker et al., 1989).

The flowmeter used during Leg 140 was designed for experiments performed on land. In the ODP case, the fluid injected into the drill pipe from pumps located onboard the ship is not ensured of entering the formation unless a packer seals the annulus between drill pipe and surface casing and, thus, prevents injected fluid from short-circuiting up into the open ocean. It is this part of the field operation which failed during the Leg 137 attempt to complete the first flowmeter/injection test conducted at sea. As a consequence, only the velocity of the fluid flow into the cased part of the hole and in front of permeable intervals was recorded in order to detect the intervals that were actually taking fluid at the time of the experiment, without constraining the fluid path with the packer. Two passes with different cable velocities, recording both on the way up and on the way down, were performed in the upper, porous and permeable section of the basement (Becker et al., 1989; Pezard, 1990).

Data Quality

Downhole data quality may be seriously degraded in excessively large diameter sections of the borehole, or by rapid changes in the hole diameter. Electrical resistivity and velocity measurements are less sensitive to such borehole effects. The nuclear measurements (density, neutron porosity, and both natural and induced spectral gamma rays) are most seriously impaired because of the large attenuation by the borehole fluid. Corrections can be applied to the original data to reduce the effects of these conditions.

Different logs may have small depth mismatches, caused by cable stretch or ship heave during recording. Small errors in depth matching can also impair the results in zones of rapidly varying lithology. To minimize such errors, a hydraulic heave compensator adjusts for ship motion in real time. Downhole data cannot be precisely matched with core data in zones where core recovery is low because of the inherently ambiguous placement of the recovered section within the interval cored.

Data Analysis

Throughout the acquisition of downhole measurements, incoming data are observed in real time on a monitor oscilloscope and simultaneously recorded on digital tape. After the completion of a set of downhole measurements, tapes are formatted to allow for shipboard analysis. The precise nature of the analysis procedure varies for each site. Although initial appraisal of the downhole data is carried out on board ship, further analyses are undertaken after the end of the leg.

Reprocessing of Downhole Data

Acoustic and Electrical Images

The BHTV images are displayed during recording, stored on a hard disk, and can subsequently be retrieved post-cruise for analysis.

The initial processing of the raw FMS data into electrical images was carried out on board ship during Leg 140 using proprietary Schlumberger software on the L-DGO VAX 3100 workstation. A dipmeter program was used to characterize the main structural fea-

tures penetrated by the borehole, with particular attention being paid to the fracture distribution. Further processing and analysis of the FMS images will be performed post-cruise in order to produce a detailed lithostratigraphy, detect, map, and identify fractures and faults, orient cores as necessary, and determine the principal horizontal stress directions in conjunction with the BHTV data.

Geochemical Measurements

Raw count rates for six elements (Ca, Si, Fe, S, Cl, and H) are obtained in real time by the Schlumberger data acquisition software. In the past, these count rates have commonly exhibited interference from chlorine; which in turn has had a particularly detrimental effect on calcium rates and to a lesser extent on the other elements. This interference is due to the dominance of the induced gamma-ray spectrum by chlorine, and can be minimized by the presence of a "boron sleeve" which suppresses the signal from the chlorine containing borehole fluids. No "boron sleeve" was present when geochemical logs were first run in Hole 504B during Leg 111, but has been standard for ODP operations since Leg 128.

The data are reprocessed after the cruise when the gamma-ray spectrum at each depth is inverted for titanium, gadolinium, and potassium in addition to the six elements listed above. Though gadolinium is present in concentrations of only a few parts per million, its neutron-capture cross section is so large that gadolinium can account for 10%–30% of the total gamma-ray intensity. Including these additional elements improve the quality of the overall inversion, particularly the accuracy of the calculated calcium abundance. The potassium concentrations determined, however, are less accurate than those from the NGT, and the K estimates from the latter are usually employed for interpretation purposes.

Aluminum concentrations from the ACT require correction for variations in cable speed. Changes in speed affect the time lag between neutron irradiation of the formation, and recording of the induced gamma-ray spectrum. Post-cruise correction for this effect is possible with techniques used in wells on land; this correction may be less reliable in ODP holes where ship heave affects the measurement in spite of mechanical compensation devices.

After geophysical and geochemical measurements have been completed, it is possible to reprocess the geochemical downhole data further. The relative abundances of Ca, Si, Fe, Ti, Al, K, S, Th, U, and Gd are used at each depth interval to calculate the photoelectric effect. The difference between this computed estimate and the actual values of the photoelectric factor as measured by the lithodensity tool may be attributed to the two major elements not directly measured, Mg and Na. As yet, no analytical method can distinguish between the relative magnitudes of these elements (Harvey et al., 1991). Once the relative elemental yields are available at the end of the spectral stripping process, the data are converted to absolute weight percent abundances. Since the source strength of the 14-MeV pulsed minitron is not known accurately, this conversion must be done indirectly through the application of an oxide closure algorithm (Herzog et al., 1987). However, this algorithm currently depends on the assumed lithology, and is therefore itself a source of errors.

Acoustic Measurements

Downhole sonic data obtained in real time are not based on full-waveform analyses but on a threshold-measuring technique that attempts to detect the compressional wave arrival by first-break criteria. Occasionally, this technique fails, and either the threshold is exceeded by noise, or the amplitude of the first compressional arrival is smaller than the threshold. The latter of these effects is known as cycle skipping and creates spurious spikes on the sonic log. Such problems may often be eliminated by reprocessing the data.

REFERENCES

- Anderson, R.N., and Zoback, M.D., 1982. Permeability, underpressures, and convection in the oceanic crust near the Costa Rica Rift, eastern equatorial Pacific. *J. Geophys. Res.*, 87:2860–2868.
- Anderson, R.N., Zoback, M.D., Hickman, S.H., and Newmark, R.L., 1985. Permeability versus depth in the upper oceanic crust: *in-situ* measurements in DSDP Hole 504B, eastern equatorial Pacific. *J. Geophys. Res.*, 90:3659–3669.
- Archie, G.E., 1942. The electrical resistivity log as an aid in determining some reservoir characteristics. *J. Pet. Tech.*, 5:1–8.
- Becker, K., Langseth, M.G., Von Herzen, R.P., and Anderson, R.N., 1983. Deep crustal geothermal measurements, Hole 504B, Costa Rica Rift. *J. Geophys. Res.*, 88:3447–3457.
- Becker, K., Sakai, H., et al., 1988. *Proc. ODP, Init. Repts.*, 111: College Station, TX (Ocean Drilling Program).
- Becker, K., Sakai, H., Merrill, R.B., Adamson, A.C., Alexandrovich, J., Alt, J.C., Anderson, R.N., Bideau, D., Gable, R., Herzig, P.M., Houghton, S., Ishizuka, H., Kawahata, H., Kinoshita, H., Lovell, M.A., Malpas, J., Masuda, H., Morin, R.H., Mottl, M.J., Pariso, J.E., Pezard, P.A., Phillips, J., Sparks, J., and Uhlig, S., 1989. Drilling deep into young oceanic crust, Hole 504B, Costa Rica Rift. *Rev. Geophys.*, 27:79–102.
- Bell, J.S., and Gough, D.L., 1979. Northeast-southwest compressive stress in Alberta: evidence from oilwells. *Earth Planet. Sci. Lett.*, 45:475–482.
- Boyce, R.E., 1976. Definitions and laboratory techniques of compressional sound velocity parameters and wet-water content, wet-bulk density, and porosity parameters by gravimetric and gamma ray attenuation techniques. In Schlanger, S.O., Jackson, E.D., et al., *Init. Repts. DSDP*, 33: Washington (U.S. Govt. Printing Office), 931–958.
- Cannat, M., Mével, C., and Stakes, D., 1991. Normal ductile shear zones at an oceanic spreading ridge: tectonic evolution of Site 735 gabbros (Southwest Indian Ocean). In Von Herzen, R.P., Robinson, P.T., et al., *Proc. ODP, Sci. Results*, 118: College Station, TX (Ocean Drilling Program), 415–429.
- Clanton, U.S., and Fletcher, C.R., 1976. Sample size and sampling errors as the source of dispersion in chemical analyses. *Proc. Lunar Sci. Conf.*, 7:1413–1428.
- Dick, H.J.B., Meyer, P.S., Bloomer, S., Kirby, S., Stakes, D., and Mawer, C., 1991. Lithostratigraphic evolution of an *in-situ* section of oceanic layer 3. In Von Herzen, R.P., Robinson, P.T., et al., *Proc. ODP, Sci. Results*, 118: College Station, TX (Ocean Drilling Program), 439–538.
- Ekstrom, M.P., Dahan, C.A., Chen, M.-Y., Lloyd, P.M., and Rossi, D.J., 1986. Formation imaging with microelectrical scanning arrays. *Trans. SPWLA 27th Annu. Logging Symp.*, Pap. BB.
- Ellis, D.V., 1987. *Well Logging for Earth Scientists*: Amsterdam (Elsevier).
- Gable, R., Morin, R.H., Becker, K., 1989. Geothermal state of Hole 504B: ODP Leg 111 overview. In Becker, K., Sakai, H., et al., *Proc. ODP, Sci. Results*, 111: College Station, TX (Ocean Drilling Program), 87–96.
- Gladney, E.S., and Roelands, I., 1988a. 1987 Compilation of elemental concentration data for USGS BHVO-1, MAG-1, QLO-1, RGM-1, SCo-1, SDC-1, SGR-1, and STM-1. *Geostand. Newsl.*, 12:253–362.
- , 1988b. 1987 Compilation of elemental concentration data for CCRMP reference rock samples SY-2, SY-3, and MRG-1. *Geostand. Newsl.*, 14:373–458.
- Harvey, P.K., Lovell, M.A., and Bristow, J.F., 1991. The interpretation of geochemical logs from the oceanic basement: mineral modeling in ODP Hole 735B. *Nucl. Geophys.*, 5:267–277.
- Hearst, J.R., and Nelson, P.H., 1984. *Well Logging for Physical Properties*: New York (McGraw-Hill).
- Herzog, R., Colson, L., Seeman, B., O'Brian, M., Scott, H., McKeon, D., Wright, P., Grau, J., Schweitzer, J., and Herron, M., 1987. Geochemical logging with spectrometry tools. *Soc. Pet. Eng., Spec. Pap.*, 16792.
- Hickman, S.H., Langseth, M.G., and Svitek, J.F., 1984. *In-situ* permeability and pore pressure measurements near the mid-Atlantic Ridge, Deep Sea Drilling Project Hole 395A. In Hyndman, R.D., Salisbury, M.H., et al., *Init. Repts. DSDP*, 78 (Pt. 2): Washington (U.S. Govt. Printing Office), 699–708.
- Jaeger, J.C., 1956. Conduction of heat in an infinite region bounded internally by a circular cylinder of a perfect conductor. *Aust. J. Physics*, 9:167–179.
- MacCaskie, D.R., 1986. Rapid field estimation of the degree of preferred orientation of elongate features. *J. Geol.*, 94:777–779.
- Morin, R., Gable, R., Becker, K., 1990. State of lithospheric stress and borehole stability at DSDP Site 504, eastern equatorial Pacific. *J. Geophys. Res.*, 95:9293–9303.
- Norrish, K., and Chappell, B.W., 1967. X-ray fluorescence spectrography. In Zussman, J. (Ed.), *Physical Methods in Determinative Mineralogy*: New York (Academic Press), 161–214.
- Norrish, K., and Hutton, J.T., 1969. An accurate X-ray spectrographic method for the analysis of a wide range of geological samples. *Geochim. Cosmochim. Acta*, 33:431–453.
- Pezard, P.A., 1990. Electrical properties of mid-ocean ridge basalts, and implications for the structure of the upper oceanic crust in Hole 504B. *J. Geophys. Res.*, 95:9237–9364.
- Pezard, P.A., Anderson, R.N., Howard, J.J., and Luthi, S.M., 1988. Fracture distribution and basement structure from measurements of electrical resistivity in the Cajon Pass scientific drillhole, California. *Geophys. Res. Lett.*, 15:1021–1025.
- Pezard, P.A., and Luthi, S.M., 1988. Borehole electrical images in the basement of the Cajon Pass scientific drillhole, California; fracture identification and tectonic implications. *Geophys. Res. Lett.*, 15:1017–1020.
- Reynolds, R.C., Jr., 1963. Matrix corrections in trace element analysis by X-ray fluorescence: estimation of the mass absorption coefficient by Compton scattering. *Am. Mineral.*, 48:1133–1143.
- , 1967. Estimation of mass absorption coefficients by Compton scattering: Improvements and extensions of the method. *Am. Mineral.*, 52:1493–1502.
- Shipboard Scientific Party, 1988a. Site 504: Costa Rica Rift. In Becker, K., Sakai, H., et al., *Proc. ODP, Init. Repts.*, 111: College Station, TX (Ocean Drilling Program), 35–251.
- , 1988b. Site 648. In Detrick, R., Honnorez, J., Bryan, W. B., Juteau, T., et al., *Proc. ODP, Init. Repts.*, 106/109: College Station, TX (Ocean Drilling Program), 35–134.
- , 1989. Site 735. In Robinson, P. T., Von Herzen, R. P., et al., *Proc. ODP, Init. Repts.*, 118: College Station, TX (Ocean Drilling Program), 89–222.
- Staudigel, H., 1979. Chemical analyses of inter-laboratory standards. In Donnelly, T., Francheteau, J., Bryan, W., Robinson, P., Flower, M., Salisbury, M., et al., *Init. Repts. DSDP*, 51, 52, 53: Washington (U.S. Govt. Printing Office), 1331–1333.
- Streckeisen, A.L., 1976. To each plutonic rock its proper name. *Earth Sci. Rev.*, 12:1–33.
- Terashima, S., and Ando, A., 1987. Elemental concentrations in nine new Japanese rock reference samples. *Geostand. Newsl.* 11:75–78.
- Thompson, G., and Bankston, D.C., 1970. Sample contamination from grinding and sieving determined by emission spectroscopy. *Appl. Spectros.*, 24:210–219.
- Vacquier, V., 1985. The measurement of thermal conductivity of solids with a transient linear heat source on the plane surface of a poorly conducting body. *Earth Planet. Sci. Lett.*, 74:275–279.
- Von Herzen, R.P., and Maxwell, A.E., 1959. The measurement of thermal conductivity of deep-sea sediments by a needle probe method. *J. Geophys. Res.*, 64:1557.
- Walker, D., 1973. Behavior of X-ray mass absorption coefficients near absorption edges: Reynold's method revisited. *Am. Mineral.*, 58:1069–1072.